THE JOURNAL OF PHYSICAL CHEMISTRY C

Article

Cite This: J. Phys. Chem. C 2019, 123, 7968−7987

pubs.acs.org/JPCC

Al Organization in the SSZ-13 Zeolite. Al Distribution and Extraframework Sites of Divalent Cations

Kinga Mlekodaj, Jiri Dedecek, Veronika Pashkova, Edyta Tabor, Petr Klein, Martina Urbanova, Robert Karcz, Petr Sazama, Sarah R. Whittleton, Haunani M. Thomas, Anna V. Fishchuk, and Stepan Sklenak*

J. Heyrovsky Institute of Physical Chemistry, The Czech Academy of Sciences, Dolejskova 3, CZ 18223 Prague 8, Czech Republic

Supporting Information

ABSTRACT: SSZ-13 is a Si-rich (Si/Al > 5) small pore zeolite (chabazite topology) important for both acid and redox catalysis. Using a sample with Si/Al = 12, a new procedure involving ^{27}Al (3Q) MAS NMR spectroscopy and extensive periodic DFT calculations with molecular dynamics, in addition to the standard methods based on bare Co(II) cations as probes monitored by FTIR spectroscopy and UV−vis spectroscopy, was employed. The placement of the Al−O−(Si−O)$_2$−Al and Al−O−(Si−O)$_3$−Al sequences in the zeolite framework was determined (Al−O−Si−O−Al sequences are absent). 54% of the framework Al atoms correspond to Al−O−(Si−O)$_3$−Al sequences which cannot form cationic sites for bare divalent cations but are able to accommodate divalent Co(II) hexaaqua complexes. The corresponding Al−O−(Si−O)$_3$−Al sequence is located in two double 6-ring cages with one Al located in the 4-ring connecting two double 6-ring units. Our study also reveals that 35% of the framework Al atoms can accommodate neither divalent Co(II) hexaaqua complexes nor bare divalent cations. Furthermore, the siting of the Al atoms of the Al−O−(Si−O)$_2$−Al and Al−O−(Si−O)$_3$−Al sequences forming four cationic sites for divalent cations located in the 6-ring (Al−O−(Si−O)$_2$−Al), 8-ring (Al−O−(Si−O)$_2$−Al and Al−O−(Si−O)$_3$−Al), and double 6-ring (Al−O−(Si−O)$_2$−Al) was determined. These Al atoms correspond to a minority of the Al framework atoms.

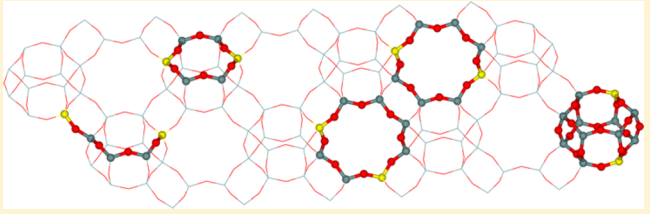

1. INTRODUCTION

Zeolites are crystalline microporous alumosilicates industrially employed as catalysts and sorbents. Their three-dimensional frameworks are made of corner-sharing SiO_4 and AlO_4^- tetrahedra. The isomorphous substitutions of Al atoms into the silicate framework result in the introduction of negative charges of AlO_4^- tetrahedra that are balanced by either protons or extraframework cationic species (metal cations and metal-oxo cations). These are the catalytic and sorption centers.

The catalytic properties of a Si-rich zeolite depend on the organization of aluminum atoms in the framework.[1] The Al organization in the SSZ-13 zeolite (Figure 1) includes the *Al distribution* (Table 1), *the siting of bare divalent cations* (Table 1) *and the Al pairs* forming the corresponding cationic sites (Table 1), and *the siting of close unpaired Al atoms* (Table 1).

The aluminum distribution controls the concentration and stability of mono- and divalent cations and metal−oxo species.[1−3] In addition, for monovalent cationic species, including protons, the aluminum distribution also controls the distance between the active sites and thus a possibility of their cooperation.[4,5] The catalytic properties can be affected by (i) the siting of Al pairs forming the cationic sites together with the siting and structure of the divalent cations occupying these cationic sites and (ii) the siting of close unpaired Al atoms which are responsible for the formation and siting of monovalent oxo-species of divalent cations.[1,5−11] Several catalytic studies have shown that zeolites of the same chemical composition but different aluminum organization could possess different catalytic properties.[1] Therefore, the potential of a zeolite for individual catalytic reactions cannot be evaluated without the knowledge of the aluminum organization in the framework.

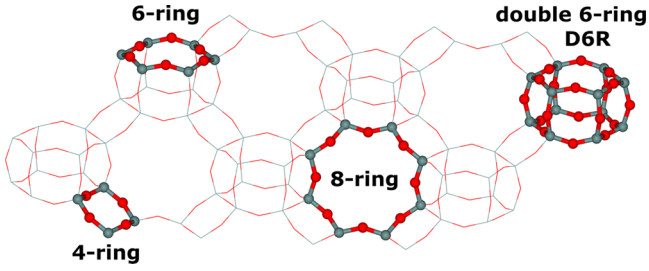

Figure 1. Structure of SSZ-13 (chabazite topology). T atoms (Si or Al) are shown in gray and oxygen atoms in red. A 4-ring, a 6-ring, an 8-ring, and a double 6-ring (D6R) are highlighted. Al atoms occupy some T sites.

Special Issue: Hans-Joachim Freund and Joachim Sauer Festschrift

Received: July 30, 2018
Revised: October 26, 2018
Published: October 29, 2018

DOI: 10.1021/acs.jpcc.8b07343
J. Phys. Chem. C 2019, 123, 7968−7987

Table 1. Definition of Terms Regarding the Al Organization

term	Definition
Al pairs (Al_{PAIR})	Two Al atoms separated by two or three Si atoms located in one 6-ring (only Al−O−(Si−O)$_2$−Al) or 8-ring (both Al−O−(Si−O)$_2$−Al and Al−O−(Si−O)$_3$−Al) and forming a cationic site for bare divalent (Co(II)) cations in dehydrated zeolites. They are also able to accommodate Co(II) hexaaqua complexes in hydrated zeolites.
Al distribution	The distribution of framework aluminum atoms among (i) Al−O−(Si−O)$_2$−Al and Al−O−(Si−O)$_3$−Al sequences in the rings forming cationic sites for bare divalent cations, (ii) Al−O−(Si−O)$_{n\geq2}$−Al sequences corresponding to close unpaired Al atoms, and (iii) single Al atoms.
close unpaired Al atoms (Al_{CLOSE})	Al atoms of Al−O−(Si−O)$_{n\geq2}$−Al sequences accommodating Co(II) hexaaqua complexes in hydrated zeolites, but not bare Co(II) cations in dehydrated zeolites.
single Al atoms (Al_{SINGLE})	These are unable to accommodate both bare Co(II) cations in dehydrated zeolites and Co(II) hexaaqua complexes in hydrated zeolites.
siting of Al pairs and close unpaired Al atoms	Locations of Al atoms of Al−O−(Si−O)$_n$−Al sequences corresponding to Al pairs and close unpaired Al atoms in the zeolite framework.
siting of bare divalent cations	Positions of bare extraframework divalent cations in 6-rings and 8-rings of the zeolite framework.
Al organization in SSZ-13	Al distribution + siting of Al pairs, close unpaired Al atoms, and bare divalent cations.

The SSZ-13 zeolite possesses the CHA topology,[12] and it is the Si-rich (Si/Al > 5) analogue of the naturally occurring zeolite chabazite (Si/Al 2) of the same CHA topology.[12] SSZ-13 is one of the most important three-dimensional small-pore zeolites since it can be entered through 8-ring windows.[13] The CHA structure features one T-site and double 6-ring (D6R) building units (Figure 1).[13] The CHA topology requires a formation of Al−O−Si−O−Al for the Si/Al ratio below 7.[14] Stacy Zones described the first viable synthesis procedure for SSZ-13.[15]

SSZ-13 attracted a lot of attention because of its extraordinary performances in various catalytic reactions such as SCR of NOx[16−23] and methanol-to-olefin (MTO)[24−26] and ethylene-to-propylene (ETP).[27] In addition, SSZ-13 exhibits excellent CO_2 adsorption properties.[28]

As the importance of the SSZ-13 zeolite rises, it induces emerging studies on the distribution of the aluminum atoms in the framework and on its influence on the catalytic stability and performance together with a possible control of the Al distribution. Deimund et al. tested a series of SSZ-13 zeolites synthesized with the increasing Si/Al ratio for the methanol to olefin reaction and observed different catalytic behavior for the samples.[25] Shorter deactivation times and lower selectivity of olefins were observed for the samples with lower Si/Al ratios (higher probability for having cooperating acid sites).[25] Several studies investigated the influence of the Al distribution in copper-exchanged SSZ-13 zeolites employed in the SCR reaction on (i) the activity of the catalysts in the low-temperature range and (ii) their hydrothermal stability. It was shown that the most favorable stabilization of the copper cations was their accommodation in the 6-ring with two Al atoms.[29−31] Zhao et al. employed ^{23}Na MQ MAS NMR spectroscopy to study the Na^+ cationic sites in SSZ-13 and inferred that there are Al−O−Si−O−Al and Al−O−Si−O−Si−O−Al sequences located in the 6-ring.[32] Atom probe tomography was used on ZSM-5 to determine the spatial distribution of individual Al atoms.[33] However, not only does this method not have the required resolution to distinguish the single Al atoms, Al pairs, and close unpaired Al atoms, but also there is only a weak relationship between the geometrical distance of Al atoms and the Al distribution. Al atoms in different rings or cavities which are unable to accommodate both bare Co(II) cations in dehydrated zeolites and Co(II) hexaaqua complexes in hydrated zeolites represent single Al atoms although they can be geometrically close. Furthermore, the differences in the geometrical distance between the Al pairs and close unpaired Al atoms can be negligible.

Di Iorio and Gounder concentrated on controlling the Al distribution by varying the ratio of cations in the crystallization medium.[34] Di Iorio et al. reported SSZ-13 zeolites with the Si/Al values from 14 to 17 and the amount of pairs from 0 to 44%.[35] However, only the ion-exchange capacity of the hydrated samples was employed to monitor the Al distribution between single Al atoms and Al pairs. Although this approach was found to be valid for ZSM-5 zeolites, ferrierites, and mordenites, it completely failed in the case of beta zeolites due to the presence of close unpaired Al atoms with significantly different properties, distinguishable from Al pairs only by UV−vis spectroscopy or FTIR spectroscopy in dehydrated zeolites (not performed by Di Iorio et al.).[1] Therefore, the concentrations of Al pairs reported by Di Iorio et al. correspond to the sum of the concentrations of the Al pairs and close unpaired Al atoms. However, the close unpaired Al atoms can prevail in SSZ-13 as the investigation of our SSZ-13 sample showed.

In this article, a new significantly improved procedure for the analysis of the Al organization in SSZ-13 is described. Our approach includes, in addition to employing the standard methods based on Co(II) cations as probes monitored by FTIR spectroscopy and UV−vis spectroscopy, also ^{27}Al (3Q) MAS NMR spectroscopy and extensive periodic DFT calculations including molecular dynamics. The Al distribution, the siting of close unpaired Al atoms, and the siting and structure of four cationic sites including the siting of the Al pairs forming these sites are presented.

SSZ-13 of the chabazite topology zeolite belongs to the ABC family which significantly differs from the family of the pentasil-ring zeolites.[13] The concept of the Al distribution and methodology of its analysis was developed on the ZSM-5 zeolite,[36,37] a typical pentasil-ring material, and later applications and improvements dealt only with other members of the pentasil-ring family (e.g., ferrierite,[38] beta zeolite,[3,39] and TNU-9[40]).[1] Therefore, the analysis of the Al distribution in other than pentasil-ring zeolite requires rethinking and redeveloping of both the concept and methodology. Moreover, the first analysis of the complete siting of divalent cations in SSZ-13 was performed. Furthermore, a new method to determine the arrangement of close unpaired Al atoms is reported.

DOI: 10.1021/acs.jpcc.8b07343
J. Phys. Chem. C 2019, 123, 7968−7987

While ^{27}Al (3Q) MAS NMR spectroscopy has been successfully employed to (partly) determine the Al siting,[38,41−43] this method is used for the first time for the analysis of the Al distribution. SSZ-13 is the first zeolite for which the structure and location in the zeolite framework of close unpaired Al atoms are determined employing ^{27}Al (3Q) MAS NMR spectroscopy in tandem with DFT calculations. Furthermore, we redefined Al pairs and single Al atoms in zeolites and described a new type of the Al organization in zeolites (not present in pentasil-ring zeolites)—two Al atoms unable to accommodate Co(II) hexaaqua complexes in hydrated zeolites but capable of accommodating bare Co(II) cations in dehydrated zeolites.

2. EXPERIMENTAL SECTION

SSZ-13 zeolite with Si/Al 12 was synthesized based on the method of Fickel et al.[44] (for details see the Supporting Information which also describes the preparations of the individual cationic forms of calcined SSZ-13). The Na-SSZ13 sample was characterized by X-ray diffraction, SEM, and ^{29}Si MAS NMR (framework aluminum content) (for details see the Supporting Information).

^{27}Al MAS NMR and ^{27}Al 3Q MAS NMR were employed to characterize the local coordination of Al atoms in the framework (for details concerning the experiments and analysis of the spectra see the Supporting Information).

FTIR spectroscopy of the dehydrated Co-exchanged samples in the region of the shifted antisymmetric T−O−T stretching vibrations of the lattice induced by binding bare Co(II) cations to the framework oxygens was employed to monitor the binding of Co(II) cations to the cationic sites (for details see the Supporting Information). Adsorption of d_3-acetonitrile monitored by FTIR served to quantify the bare Co(II) cations accommodated in the cationic sites (for details see the Supporting Information).

The complementary method used for the analysis of the bare Co(II) cations located in Co-SSZ-13 was UV−vis diffuse reflectance spectroscopy of dehydrated Co-exchanged samples (for details see the Supporting Information).

3. REFINEMENT OF THE CONCEPT OF THE AL DISTRIBUTION FOR SSZ-13

The Al distribution was first investigated and defined for pentasil-ring zeolites (e.g., ZSM-5, the beta zeolite, mordenite, ferrierite, and TNU-9).[1,3,7,12,36−38,40] However, since the framework of SSZ-13 is composed exclusively of combinations of 4-rings, 6-rings, and 8-rings and the walls of SSZ-13 zeolite are formed by a single layer of TO_4 tetrahedra facing simultaneously several cavities,[12] a detailed discussion of the concept of the Al distribution in SSZ-13 is required. This discussion should respect a possible need of the refinement of the definition of various Al species for the case of SSZ-13. Furthermore, the relationship of the properties relevant to catalysis (e.g., the proximity of acid sites, the siting of extra-framework divalent cations, and the application of Co(II) cations as a probe of the Al organization) to the Al distribution should be included as well.

3.1. Cationic Sites in SSZ-13. According to XRD studies concluded by Mortier, there are three cationic sites reported for bare cations in the chabazite zeolite: the 6-ring of the hexagonal prism (D6R), sites B or C according to Mortier; the 8-ring, site D; and the cation location inside the D6R unit, site A.[45−48] Nevertheless, this notation represents only the geometry of the site and does not take into account the Al distribution in the site. While the differences in the siting of mono- and divalent cations in the case of Al-rich zeolites result only from the size of the ring, the Al distribution should play a significant role for Si-rich materials for which the presence of two Al atoms in each ring or site is not guaranteed. Therefore, cationic sites formed by two Al atoms for divalent cations in the Si-rich SSZ-13 zeolite are defined as follows (see also Section 5): the ω site inside the hexagonal prism of the D6R, the σ site in the 6-ring, and the τ site in the 8-ring (Figure 2).[45−48]

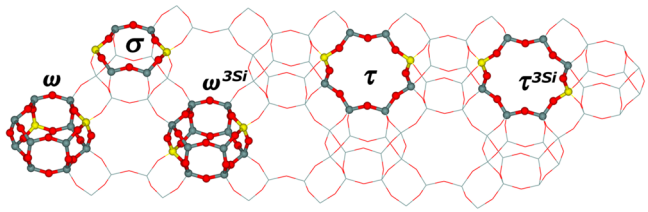

Figure 2. Structure of the empty σ, τ, τ^{3Si}, ω, and ω^{3Si} cationic sites in the SSZ-13 zeolite. Silicon atoms are in gray, oxygen atoms in red, and aluminum atoms in yellow.

3.2. Al−O−Si−O−Al Sequences. These Al species are well-known for Al-rich zeolites in which they significantly predominate.[49−52] However, they were also reported for ZSM-5 and the beta zeolite.[3,53,54] The Al−O−Si−O−Al sequences are arranged in these matrices in such a way that each Al atom is facing a different channel.[3,53] The two Al atoms of Al−O−Si−O−Al in ZSM-5 and the beta zeolites exhibit a behavior of single Al atoms both regarding the cooperation of two acid sites (i.e., the two sites are noncooperating) as well as the accommodation of divalent cationic structures (i.e., these two Al atoms are not able to accommodate bare Me(II) cations).

Conversely, the two Al atoms of Al−O−Si−O−Al in SSZ-13 face the same cavity, and therefore they exhibit the properties of Al−O−Si−O−Al species in Al-rich zeolites (a possible cooperation of two Al-related acid sites and a stabilization of both divalent cation complexes and bare divalent cations). Nevertheless, the definition of Al−O−Si−O−Al sequences does not have to be revised. The Al−O−Si−O−Al sequences can be monitored by ^{29}Si MAS NMR spectroscopy since their presence in the zeolite framework is reflected in the existence of ^{29}Si NMR resonances corresponding to Si(2Si,2Al) atoms in the spectrum. Depending on the Al−O−Si−O−Al siting in the zeolite framework, the Al−O−Si−O−Al species are able to accommodate divalent Co(II) hexaaqua complexes and bare Co(II) cations (Al−O−Si−O−Al in 6-rings and 8-rings of the SSZ-13 framework).

3.3. Al Pairs in SSZ-13 (Al_{PAIR}). Cationic sites for extra-framework bare divalent cations in zeolites were suggested to represent Al pairs, i.e., two Al atoms separated by two Si atoms (i.e., Al−O−$(Si−O)_2$−Al) located in one 6-ring accommodating bare Co(II) cations in dehydrated zeolite.[2,3,38−40,53,55−59] The σ cationic site in the 6-ring can be formed only by Al−O−$(Si−O)_2$−Al sequences (Figure 2), while the τ and ω sites in the 8-ring and D6R, respectively, can be created by both Al−O−$(Si−O)_2$−Al and Al−O−$(Si−O)_3$−Al sequences (Figure 2) analogously to the β site in mordenite.[60] Therefore, the definition of Al pairs in Si-rich zeolites has to be extended to include both Al−O−$(Si−O)_2$−Al and Al−O−$(Si−O)_3$−Al

DOI: 10.1021/acs.jpcc.8b07343
J. Phys. Chem. C 2019, 123, 7968−7987

sequences; i.e., *Al pairs (Al_{PAIR}) represent two Al atoms separated by two or three Si atoms located in one 6-ring (only Al−O−(Si−O)$_2$−Al) or 8-ring (both Al−O-(Si−O)$_2$-Al and Al−O-(Si−O)$_3$-Al) and forming a cationic site for bare divalent (Co(II)) cations in dehydrated zeolites. Moreover, they are also able to accommodate Co(II) hexaaqua complexes in hydrated zeolites. The acid sites in protonic zeolites related to Al pairs can cooperate.* It should be pointed out that the extension of Al pairs to Al−O−(Si−O)$_3$−Al in 8-rings requires a further confirmation regarding the separation of two Al atoms by three Si atoms and concerning the formation of cationic sites for bare Co(II) cations.

3.4. Close Unpaired Al Atoms (Al_{CLOSE}) and Single Al Atoms (Al_{SINGLE}). Close unpaired Al atoms correspond to two Al atoms capable of accommodating Co(II) hexaaqua complexes in hydrated zeolites but unable to accommodate bare Co(II) cations in dehydrated zeolites. Close unpaired Al atoms were assumed to correspond to Al−O−(Si−O)$_{n\geq 2}$−Al sequences located in two different rings. This Al species is unique for beta zeolites as revealed in several studies which reported monovalent Co(III)-oxo species to be accommodated by close unpaired Al atoms in dehydrated zeolites.[3,6,7,61] Nothing is known about such close unpaired Al atoms in SSZ-13. They may be formed by Al−O−(Si−O)$_{n\geq 2}$−Al sequences located in different rings of two hexagonal prisms (D6R). It should be noted that the distances of Al in Al−O−(Si−O)$_n$−Al sequences with $n \gg 2$ can be relatively short in cavities of the SSZ-13 structure, and such Al atoms can still accommodate Co(II) hexaaqua complexes. The possibility of a cooperation of the related acid sites for each type of these Al species depends on the distance of Al atoms and the location of protons on the individual O atoms of the AlO_4^- tetrahedra. *Close unpaired Al atoms (Al_{CLOSE}) represent Al atoms of Al−O−(Si−O)$_{n\geq 2}$−Al sequences accommodating Co(II) hexaaqua complexes in hydrated zeolites but not bare Co(II) cations in dehydrated zeolites.*

There is one additional type of cationic sites in the CHA framework, well-known also for Al-rich zeolites of the faujasite structure.[45,47] This ω site (Figure 2) is present inside the hexagonal prism of the D6R (site A according to Mortier)[45−48] and accommodates a divalent cation between the two 6-rings. Each of the two 6-rings of D6R creating the ω site must possess one Al atom. These two Al atoms form either an Al−O−(Si−O)$_2$−Al or Al−O−(Si−O)$_3$−Al sequence (Figure 2) in the Si-rich SSZ-13 zeolite (assuming there are no Al−O−Si−O−Al chains present in the SSZ-13 framework). Therefore, the two Al atoms of the ω site do not fit into the definition of the Al pairs (accommodation of Co(II) hexaaqua complexes in hydrated zeolites and cooperation of the corresponding acid sites) and will be designated as *Al−O−(Si−O)$_2$−Al and Al−O−(Si−O)$_3$−Al sequences in the D6R* (i.e., hexagonal prism), in the shortened form *Al−O−(Si−O)$_2$−Al^{D6R} and Al−O−(Si−O)$_3$−Al^{D6R}. They accommodate bare Co(II) cations in dehydrated zeolites, but their two Al atoms are separated, facing two different cavities* (the only case of separated Al atoms in SSZ-13) and *are unable to accommodate Co(II) hexaaqua complexes in hydrated zeolites.* Moreover, *the acid sites related to these Al−O−(Si−O)$_2$−Al^{D6R} and Al−O−(Si−O)$_3$−Al^{D6R} sequences cannot cooperate* due to the fact that they face either two different cavities or the interior of the strictly limited space of the hexagonal prism. Therefore, when discussing acid-catalyzed reactions, *Al−O−(Si−O)$_2$−Al^{D6R} and Al−O−(Si−O)$_3$−Al^{D6R}* sequences represent single Al atoms, while in the case of redox catalysis, divalent cations in this site should not be considered since they are inaccessible for guest molecules (accessed exclusively through 6-rings).

Single Al atoms in zeolites represent Al atoms either located far enough or separated by a zeolite wall that they cannot accommodate Co(II) hexaaqua complexes in hydrated zeolites.[1,36,37] Moreover, single Al atoms are unable to accommodate bare divalent cations in dehydrated zeolites, and the corresponding acid sites cannot cooperate. Taking into account Al−O−(Si−O)$_2$−Al^{D6R} and Al−O−(Si−O)$_3$−Al^{D6R} atoms, which might be able to accommodate bare Co(II) cations, the definition of single Al atoms has to be extended. *Single Al atoms (Al_{SINGLE}) are unable to accommodate both bare Co(II) cations in dehydrated zeolites and Co(II) hexaaqua complexes in hydrated zeolites, and moreover, the corresponding acid sites cannot cooperate.* It should be noted that the Al atoms of the Al−O−(Si−O)$_2$−Al^{D6R} and Al−O−(Si−O)$_3$−Al^{D6R} would behave as isolated acid sites when facing different cavities.

4. COMPUTATIONAL MODELS AND METHODS

4.1. Calculations of Co(II) Cationic Sites. *4.1.1. Computational Models.* Five models possessing *P*1 symmetry were employed. They feature one unit cell of SSZ-13 with two Al/Si substitutions forming the possible σ, τ, τ^{3Si}, ω, and ω^{3Si} cationic sites accommodating one Co(II) cation. The starting monoclinic structure was downloaded from the zeolite structural database.[13]

4.1.2. Electronic Structure Calculations. Periodic DFT calculations were carried out by employing the VASP code[62−65] (for details see the Supporting Information).

4.1.3. Molecular Dynamics. The molecular dynamics (MD) simulations were carried out on all the five models. The simulations were run for 10 000 fs at 400 K (for details see the Supporting Information).

Visual inspection of the structures along the MD trajectories showed that the duration of the MD simulations was long enough because it included both the rearrangements of the local structures of the SSZ-13 framework (up to ca. 1000 fs) as well as a long period (ca. 9000 fs) when the system fluctuated around the equilibrium and "snapshots" were collected and optimized. Similar time lengths were used for MD simulations of cationic sites in zeolites.[2,3,8,40,66] The structures of 20 distinct "snapshots" collected at 500, 1000, 1500, ···, 10 000 fs of the molecular dynamics simulations were optimized for the computational models. Our MD approach to calculate possible rearrangements of the cationic sites upon binding divalent Co(II) cations was validated experimentally on Co(II)-ferrierite;[2] however, other approaches can also be viable.

4.1.4. Geometry Optimizations. The collected "snapshots" were optimized (for details see the Supporting Information).

4.2. Computations of ^{27}Al Isotropic Chemical Shifts. *4.2.1. Computational Models.* A bare zeolite framework model possessing *P*1 symmetry and featuring one unit cell of SSZ-13 including neither cations nor water molecules is adopted to calculate the local structure around the AlO_4^- tetrahedra and to predict the ^{27}Al NMR shielding. The bare zeolite framework model has been successfully employed in our previous studies.[38,42,53,66−72] Each Al atom bears a formal charge of −1. The starting structure was downloaded from the zeolite structural database.[13]

36 models featuring a single Al atom in all possible 36 T sites of the SSZ-13 framework were used. In addition, five

DOI: 10.1021/acs.jpcc.8b07343
J. Phys. Chem. C 2019, 123, 7968−7987

more models with two Al atoms corresponding to empty σ, τ, τ^{3Si}, ω, and ω^{3Si} cationic sites were employed as well.

Moreover, six more models featuring possible locations of two Al_{CLOSE} atoms were also used. All structures featuring Al−O−(Si−O)$_2$−Al, Al−O−(Si−O)$_3$−Al, and Al−O−(Si−O)$_4$−Al sequences with the two Al atoms located in two different hexagonal prisms (D6R) and arranged in such a way that the two Al atoms can accommodate Co(II) hexaaqua complexes in hydrated zeolites but not bare Co(II) cations in dehydrated zeolites were calculated. The corresponding structures of the six models are shown in Section 5.2.3.

For models featuring two Al atoms, the calculations were carried out for three variants of the model. Both the Al atoms (Al_I−O−(Si−O)$_n$−Al_{II}) (n = 2, 3, and 4) are present in the first variant, while Al_{II} and Al_I are replaced by Si in the second and third variants (i.e., Al_I−O−(Si−O)$_n$−Si_{II} and Si_I−O−(Si−O)$_n$−Al_{II}, respectively), respectively. Using the three variants of each model is discussed in detail elsewhere.[38,53,72]

4.2.2. Electronic Structure Calculations and Geometry Optimizations. The CP2K program was employed[73,74] to fully relax the zeolite unit cells (lattice parameters and geometries) using the BLYP functional,[75,76] GTH pseudopotentials,[77,78] and the TZV2P-GTH basis set.

4.2.3. Calculations of ^{27}Al NMR Shielding. Clusters of seven coordination shells around the Al atom of interest (Al−O−Si−O−Si−O−Si−O−H_{link}) for the 36 models featuring a single Al atom were extracted from the fully relaxed structures to calculate the ^{27}Al NMR shielding by the gauge-independent atomic orbital method (GIAO)[79] using Gaussian09,[80] the B3LYP functional,[76,81] and the pcS basis sets of Jensen[82]-pcS-4 for the Al atom of interest and pcS-1 for all the other atoms. Similarly, double centered clusters around (i) the two Al atoms of interest (Al_I−O−(Si−O)$_n$−Al_{II}), (ii) the Al_I and Si_{II} (Al_I−O−(Si−O)−Si_{II}) atoms, and (iii) the Si_I and Al_{II} (Si_I−O−(Si−O)$_n$−Al_{II}) atoms, having seven coordination shells, were used for the computational models of the cationic sites as well as $\mathbf{Al_{CLOSE}}$ atoms. The calculated ^{27}Al shielding values were converted to ^{27}Al isotropic chemical shifts using two observed ^{27}Al NMR resonances of the SSZ-13 zeolite of the Si/Al ratio of 38.[69]

5. COMPUTATIONAL RESULTS

5.1. Structures and Stability of the σ, τ, and ω Cationic Sites. Our MD calculations and the subsequent optimizations of the four models (σ, τ, τ^{3Si}, and ω) of the cationic sites of Co-SSZ-13 yielded the structures of the corresponding cationic sites, the relative binding energies[2,40] of Co(II) in these sites, and the stabilization energies[2,8,40] of the cationic sites accommodating Co(II) (Table 2).

Conversely, our MD computations of the ω^{3Si} model revealed that $Al{-}O{-}(Si{-}O)_3{-}Al^{D6R}$ sequences do not form a cationic site for divalent cations. The Co(II) cation moved to one of the two 6-rings forming the D6R during the MD simulation. Such Co(II) cations are very unstable since their two plus charge is compensated only by one minus charge of one AlO_4^- tetrahedron in the 6-ring accommodating Co(II).[83,84]

Our MD simulations of the σ and τ^{3Si} models and subsequent optimizations of selected MD snapshots led to energy stabilizations by 9 and 5 kcal mol^{-1}, respectively (Table 2), relative to the same models that were not relaxed employing MD simulations but simply optimized by using the structure downloaded from the zeolite structural database.[13] The computational results show the proper binding of Co(II) mainly to the oxygen atoms of the AlO_4^- tetrahedra and significant rearrangements of the local structures of the zeolite framework of the σ and τ^{3Si} cationic sites. Conversely, there is no rearrangement observed for the τ and ω sites (Table 2).

Table 2. Relative Binding Energies in kcal/mol of Co(II)[2,40] and Stabilization Energies[2,8,40] in kcal/mol

cationic sites	ΔBE_{Co} [a]	ΔE_{stab} [b]
σ	0.0	8.6
τ	43.0	0.1
τ^{3Si}	56.5	5.1
ω	35.0	0.0

[a]The difference between the energies of the Co-SSZ-13 featuring the site of interest and the Co-SSZ-13 with the most stable site (i.e., σ). This energy gap is corrected by subtracting the difference between the energies of the SSZ-13 with the empty site of interest and the SSZ-13 featuring the most stable site without the cation. The empty sites have two aluminum atoms in the corresponding ring forming the cationic sites that are not compensated by any cation. [b]The difference between the energies of the model relaxed by MD simulations and, subsequently, optimized and the model that was not relaxed by MD simulations but simply optimized using the starting structure downloaded from the zeolite structural database.[13]

The computational results (Table 2) also revealed the relative binding energies of Co(II) in the calculated cationic sites. The cation binds the most tightly in the σ site, followed by in the ω site, and followed by in the τ site. The binding is the weakest in the τ^{3Si} site. The optimized structures of the four models are shown in Figure 3.

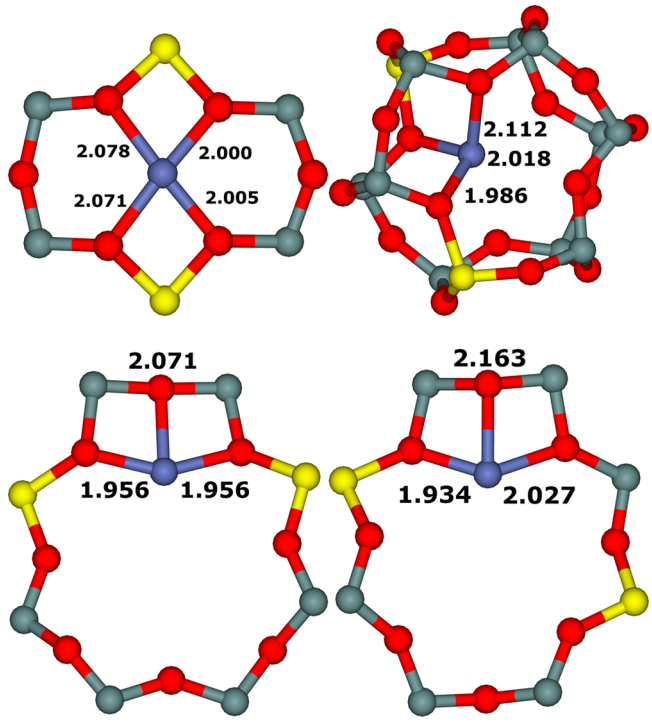

Figure 3. Optimized structures of the σ (left, top), ω (right, top), τ (left, bottom), and τ^{3Si} (right, bottom) models. The distances are in Å. Silicon atoms are in gray, oxygen atoms in red, aluminum atoms in yellow, and the cobalt atoms in blue.

DOI: 10.1021/acs.jpcc.8b07343
J. Phys. Chem. C 2019, 123, 7968−7987

The Co−O_{Al} and Co−O_{Si} bond lengths (Figure 3) range from 1.934 to 2.078 Å and from 2.027 to 2.163 Å, respectively. The calculated Co−O bond lengths are in good agreement with those obtained by EXAFS measurements, which revealed two Co−O distances of 1.99 and 2.09 Å for Co-ferrierite with Co(II) located mainly in the β sites.[59]

5.2. ^{27}Al Isotropic Chemical Shifts. *5.2.1. SSZ-13 with One Al Atom.* Our calculations employing one isolated Al atom per unit cell yielded three ^{27}Al NMR shielding values of 507.8, 508.9, and 509.1 ppm in agreement with our previous study.[69] The ^{27}Al NMR shielding of 507.8 ppm is assigned to the observed ^{27}Al isotropic chemical shift of 60.0 ppm,[69] while the other two ^{27}Al NMR shieldings are attributed to the other observed ^{27}Al NMR resonance at 59.2 ppm.[69] These relationships were used to convert the ^{27}Al NMR shielding values into ^{27}Al isotropic chemical shifts for the calculated models of the cationic sites and close unpaired Al atoms.

5.2.2. SSZ-13 Featuring the Empty Cationic Sites. The calculated ^{27}Al NMR shieldings of the five computational models are listed in Table S1 of the Supporting Information. The corresponding converted ^{27}Al isotropic chemical shifts are revealed in Table S1 of the Supporting Information and Figures 4 and 5.

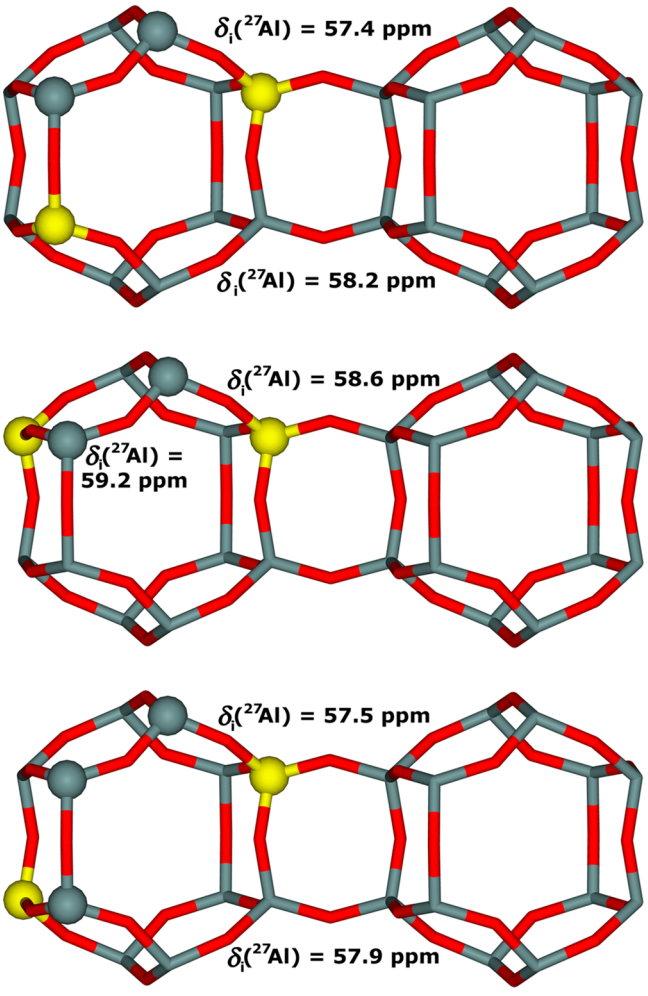

Figure 4. Structures corresponding to the empty σ (top), ω (middle), and ω^{3Si} (bottom) cationic sites and the ^{27}Al isotropic chemical shifts of the two Al atoms forming these cationic sites. Silicon atoms are in gray, oxygen atoms in red, and aluminum atoms in yellow.

Our computational results reveal that the ^{27}Al isotropic chemical shifts of the Al atoms forming the four cationic sites are changed the least for the τ and ω cationic sites (less than −1 ppm), while the largest change is obtained for the τ^{3Si} site (−3.3 ppm).

5.2.3. SSZ-13 Featuring the Al_{CLOSE} Atoms. The calculated ^{27}Al NMR shieldings of the six computational models are listed in Table S2 of the Supporting Information. The corresponding converted ^{27}Al isotropic chemical shifts are shown in Table S2 of the Supporting Information and in Figure 6.

Our calculations reveal that the ^{27}Al isotropic chemical shifts of the close unpaired Al atoms are smaller by 1−2 ppm than those of the corresponding single Al atoms for most of the models. The exception is the E model which features Al atoms having their ^{27}Al isotropic chemical shift of about 61 ppm.

6. EXPERIMENTAL RESULTS

6.1. Sample. The obtained XRD pattern (Figure S1 of the Supporting Information) complies with the reference pattern for the SSZ-13 material, and no additional reflexes were observed.[85] The SEM images (Figure S2 of the Supporting Information) evidenced a highly crystalline zeolite with the crystals in the range of the crystal sizes from 0.3 to 0.5 μm. The chemical analysis of the zeolite sample yielded the Si/Al ratio of 12. The chemical composition of the prepared set of Co,Na-SSZ-13 and Co,NH_4-SSZ-13 samples obtained from the chemical analysis using the XRF method is listed in Table 3.

6.2. ^{29}Si MAS NMR Spectroscopy. The ^{29}Si MAS NMR spectrum of the SSZ-13 sample (Figure 7) is similar to those already reported in the literature.[69,86,87]

Our simulation of the ^{29}Si MAS NMR spectrum revealed four ^{29}Si NMR resonances at −98.5, −101.5, −105.0, and −111.0 ppm. ^{29}Si NMR resonances with the ^{29}Si chemical shifts between −92 and −100 ppm reflect Si(3Si,1OH) or Si(2Si,2Al) atoms. The significant increase of the ^{29}Si NMR resonance at −98.5 ppm in the cross-polarization experiment (not shown in the figures) suggests that the measured ^{29}Si NMR resonance at −98.5 ppm can be assigned to Si(3Si,1OH) atoms. Since ^{29}Si NMR resonances between −97 and −107 ppm correspond to Si(3Si,1Al) atoms and only the region above −100 ppm increased in the cross-polarization experiment, the observed ^{29}Si NMR resonances at −101.5 and −105.0 ppm were assigned to Si(3Si,1Al). ^{29}Si NMR resonances below −110 ppm reflect Si(4Si,0Al) atoms. Therefore, the ^{29}Si NMR resonance at −111.0 ppm belongs to Si(4Si,0Al) atoms. This assignment is confirmed by an excellent agreement between the Si/Al ratio of 12 obtained from the chemical analysis and the Si/Al_{FR} ratio of 12.0 received from the ^{29}Si MAS NMR spectrum employing eq 1. The above interpretation confirms that Si(2Si,2Al), Si(1Si,3Al), and extra framework Al atoms are not present in the investigated zeolite.

$$Si/Al_{FR} = I/0.25I_1 \quad (1)$$

where I denotes the total intensity of the ^{29}Si NMR signal in the single-pulse experiment and I_1 denotes the intensity of the NMR line corresponding to the Si(3Si,1Al) atoms (Section S2.2. of the Supporting Information).

6.3. ^{27}Al (3Q) MAS NMR Spectroscopy. ^{27}Al MAS NMR single-pulse spectrum of the hydrated Na-SSZ-13 is shown in Figure 8a.

The spectrum exhibits a signal only in the region of tetrahedral framework Al atoms. ^{27}Al NMR resonances at

DOI: 10.1021/acs.jpcc.8b07343
J. Phys. Chem. C 2019, 123, 7968−7987

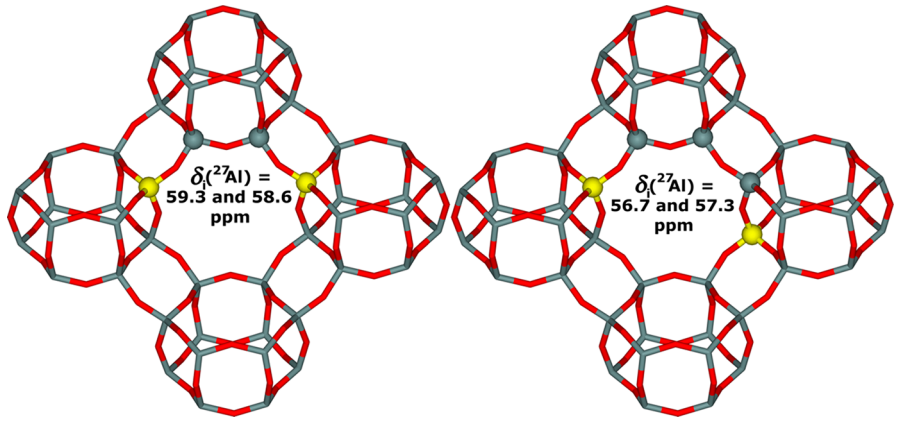

Figure 5. Structures corresponding to the empty τ (left) and τ^{3Si} (right) cationic sites and the ^{27}Al isotropic chemical shifts of the two Al atoms forming these cationic sites. Silicon atoms are in gray, oxygen atoms in red, and aluminum atoms in yellow.

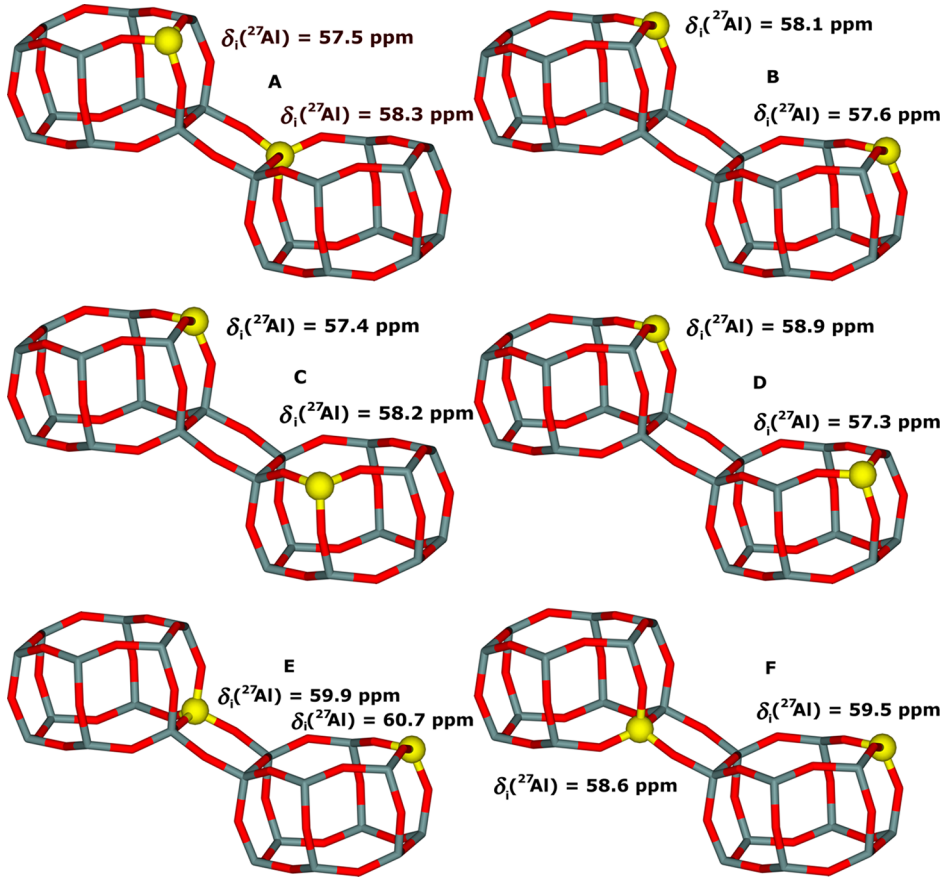

Figure 6. Structures corresponding to possible close unpaired Al atoms and their corresponding ^{27}Al isotropic chemical shifts. Silicon atoms are in gray, oxygen atoms in red, and aluminum atoms in yellow.

Table 3. Chemical Composition and the Conditions of the Preparation of the Co,Na-SSZ-13 and Co,NH_4-SSZ-13 Samples

sample	Co/Al	Co mmol/g	Na/Al	Na mmol/g	Co in solution mol/L	solution/1 g zeolite mL/g	time/h
Co,Na-SSZ-13/a	0.33	0.42	0.04	0.05	0.05	100	72
Co,Na-SSZ-13/b	0.18	0.33	0.02	0.03	0.03	100	48
Co,Na-SSZ-13/c	0.09	0.11	0.28	0.34	0.01	100	24
Co,Na-SSZ-13/d	0.02	0.02	0.30	0.36	0.01	100	12
Co,NH_4-SSZ-13/e	0.24	0.31	0.03	0.04	0.05	100	72
Co,NH_4-SSZ-13/f	0.18	0.23	0.02	0.03	0.03	100	48
Co,NH_4-SSZ-13/g	0.06	0.07	0.00	-	0.01	100	24
Co,NH_4-SSZ-13/h	0.02	0.02	0.00	-	0.01	100	12

DOI: 10.1021/acs.jpcc.8b07343
J. Phys. Chem. C 2019, 123, 7968−7987

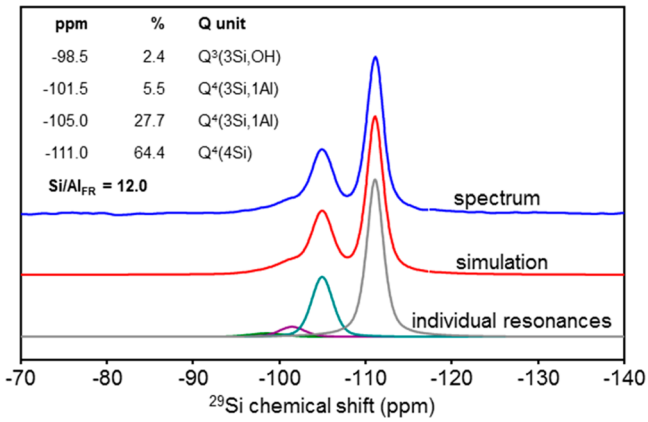

Figure 7. ^{29}Si MAS NMR spectrum of the Na-SSZ-13 sample and the simulation of the spectrum with Gaussian bands of the individual resonances.

around 0 ppm as well as between 15 and 30 ppm corresponding to extra-framework octahedral and pentacoordinated Al atoms, respectively, were not observed. This confirms the exclusive presence of tetrahedral framework Al atoms in the zeolite.

Unexpectedly, although the CHA topology contains only one crystallographically distinguishable framework T site, the ^{27}Al MAS NMR spectrum of SSZ-13 is rather broad. Visual inspection reveals at least two ^{27}Al NMR resonances. Our prior study of the Si-rich SSZ-13 (Si/Al 38) zeolite revealed that Al/Si substitutions caused the splitting of the single T site into three T sites having slightly different local geometries.[69] However, the corresponding splitting of the ^{27}Al isotropic chemical shift is very small (0.8 ppm)[69] and cannot itself explain the observed spectrum. The variability of the AlO_4^- local geometries due to the different arrangements of various Al−O−(Si−O)$_n$−Al sequences in the SSZ-13 framework is most likely responsible for the broadness of the ^{27}Al MAS NMR spectrum. It should be noted that the presence of Al atoms as the next-nearest and next-next-nearest neighbors has already been shown to affect the geometry of the AlO_4^- tetrahedron and ^{27}Al NMR parameters.[53,69] Our DFT calculations of the ^{27}Al NMR parameters of Al atoms located in different Al−O−(Si−O)$_n$−Al sequences (Tables S1 and S2 of the Supporting Information and Figures 4−6) reveal a relatively broad variability of the predicted ^{27}Al isotropic chemical shifts lying in the range from 56.7 to 60.7 ppm. This variability is most likely responsible for the shape of the spectrum of Na-SSZ-13. It should be noted that also the quadrupolar broadening of individual ^{27}Al NMR resonances and the presence of other transitions than those between the −1/2 and 1/2 states can affect the shape of the spectrum.[88] Therefore, the exact analysis of the spectrum requires a combination of multiple quantum experiments (analysis of the number of ^{27}Al NMR resonances and their parameters) with the single-pulse measurement (quantitative analysis of the concentrations of the individual Al species is possible only for single-pulse spectra).

On-sight analysis of the ^{27}Al 3Q MAS NMR spectrum depicted in Figure 8b confirms the presence of at least two ^{27}Al NMR resonances in the spectrum of the Na-SSZ-13 sample. Detailed analysis employing a simulation of the 2D spectrum confirmed the presence of two broad ^{27}Al NMR resonances with the ^{27}Al isotropic chemical shifts of 59.4 and 60.0 ppm. The corresponding concentrations of the Al atoms obtained from the single-pulse ^{27}Al MAS NMR measurements are 75 and 25%, respectively.

The broadening of both the ^{27}Al NMR resonances originates from either the variability of the middle-range and long-range orderings of the zeolite framework due to various isomorphous substitutions of Al into the zeolite framework or the presence of other ^{27}Al NMR resonances with close NMR parameters. It should be noted that the spectrum simulation represents the result with the lowest number of ^{27}Al NMR resonances required to obtain an acceptable simulation of the signal. Nevertheless, simulations of the spectrum with varied ^{27}Al isotropic chemical shifts clearly showed that there were ^{27}Al NMR resonances neither above 60.0 ppm nor below 58.0 ppm in the spectrum.

6.4. FTIR of Adsorbed d_3-Acetonitrile. The spectra of d_3-acetonitrile adsorbed on the series of Co,H-SSZ-13 and Co,Na-SSZ-13 are depicted in Figure 9.

Five bands are recognizable in the spectra: band at 2323 cm^{-1} attributed to framework aluminum Lewis sites, vibration at 2309 cm^{-1} corresponding to Lewis acid sites of bare cobalt cations, band at 2282 cm^{-1} reflecting sodium cations, vibration at 2298 cm^{-1} related to Brønsted sites, and band at 2253 cm^{-1} assigned to d_3-acetonitrile physisorbed on the surface of the

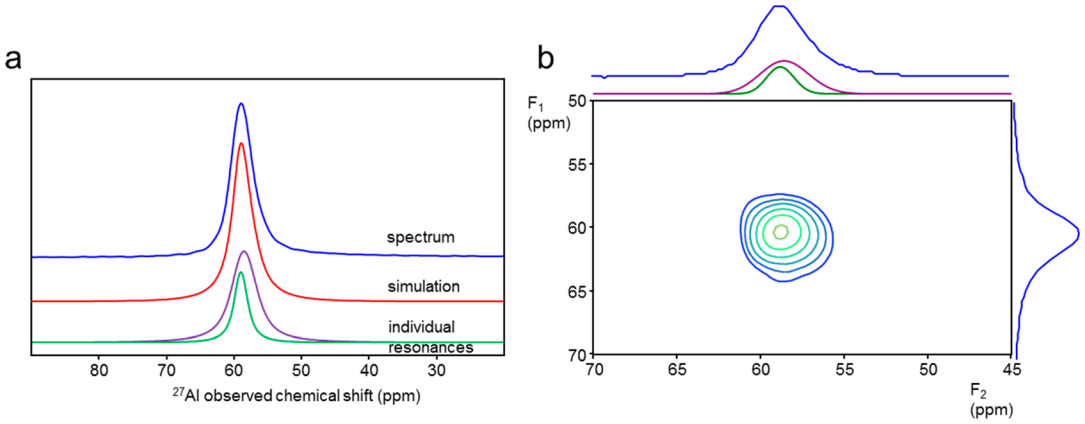

Figure 8. ^{27}Al MAS NMR spectrum of the Na-SSZ-13 sample, a simulation of the spectrum with the individual ^{27}Al NMR resonances (a). The 2D plot of the ^{27}Al 3Q MAS NMR spectrum of the Na-SSZ-13 sample, the F_1 and F_2 projections (blue), and a simulation of the individual resonances in the F2 projection (violet and green) (b).

DOI: 10.1021/acs.jpcc.8b07343
J. Phys. Chem. C 2019, 123, 7968−7987

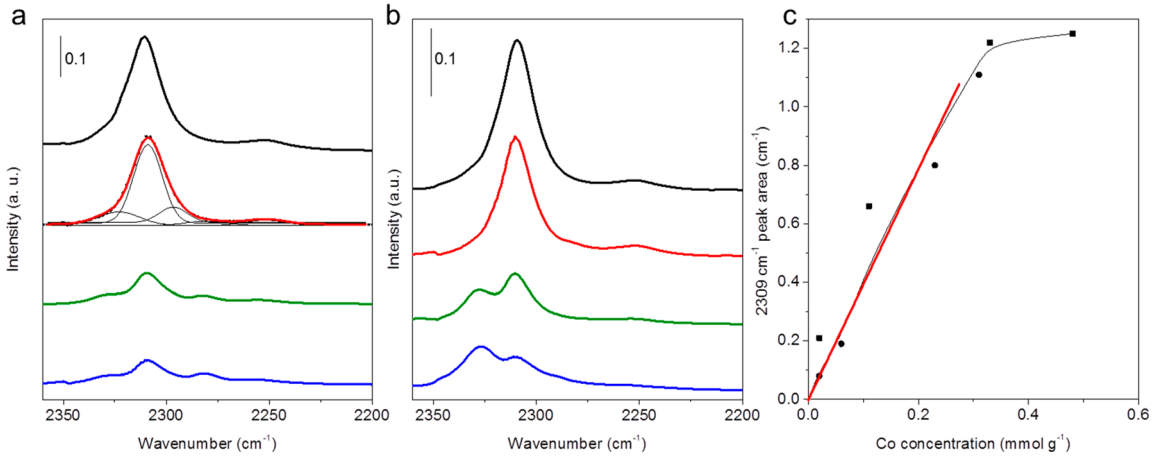

Figure 9. FTIR spectra of d_3-acetonitrile adsorbed on the series of Co,Na-SSZ-13 (a–d, black, red, green, and blue, respectively, lines) with a simulation of the spectrum of Co,Na-SSZ-13/b (●●●) and the individual Gaussian bands and Co,H-SSZ-13 (e–h, black, red, green, and blue, respectively, lines) (a) and (b), respectively, and the effect of the Co loading on the integrated area of the maximum at 2309 cm^{-1} for the Co,Na-SSZ-13 series (■) and Co,H-SSZ-13 series (●) (c).

sample. The integrated area of the band related to the Lewis acid sites of bare cobalt cations showed a linear dependence in lower cobalt concentrations, while there is a plateau at the highest Co loadings. This result allowed us to estimate the extinction coefficient of d_3-acetonitrile adsorbed on Co(II) which is shown in Table 4 and compared with the data known for other zeolites.

Table 4. Extinction Coefficients of d_3-Acetonitrile Adsorbed on Bare Co(II) Cations and the Shifted Antisymmetric T–O–T Stretching Lattice Modes of the Zeolite Framework Induced by Binding Bare Co(II) Cations

	extinction coefficient ($cm \cdot \mu mol^{-1}$)			
spectrum	SSZ-13	beta zeolite[89]	ferrierite	TNU-9[40]
d_3-acetonitrile	4.5	7.12	-	11
T–O–T vibrations	30.0	-	38.2	

6.5. FTIR of the Shifted Antisymmetric T–O–T Stretching Vibrations. The FTIR spectra (Figure 10) of the dehydrated series of the Co,H-SSZ-13 and Co,Na-SSZ-13 samples in the region of the shifted antisymmetric T–O–T stretching lattice modes of the zeolite framework induced by binding bare Co(II) cations to the framework oxygens (960–880 cm^{-1}) confirmed the presence of bare cobalt cations accommodated in the cationic sites.

Since the total area of the vibrations increased linearly with the rising concentration of Co(II) cations in the samples with lower Co loadings, the determination of the extinction coefficient for this region was possible (Figure 10c). The extinction coefficient is also given in Table 4 and compared with those of other zeolites. Conversely, the intensity of the shifted antisymmetric T–O–T stretching lattice modes reached a constant value for higher Co(II) loadings. It is possible to distinguish four maxima: three at 895, 907, and 924 cm^{-1} for all the samples in the entire range of concentrations and one more maximum at 948 cm^{-1} only for high concentrations of Co(II). The simulation of the spectrum is shown in Figure 11a, and the corresponding wavenumbers of

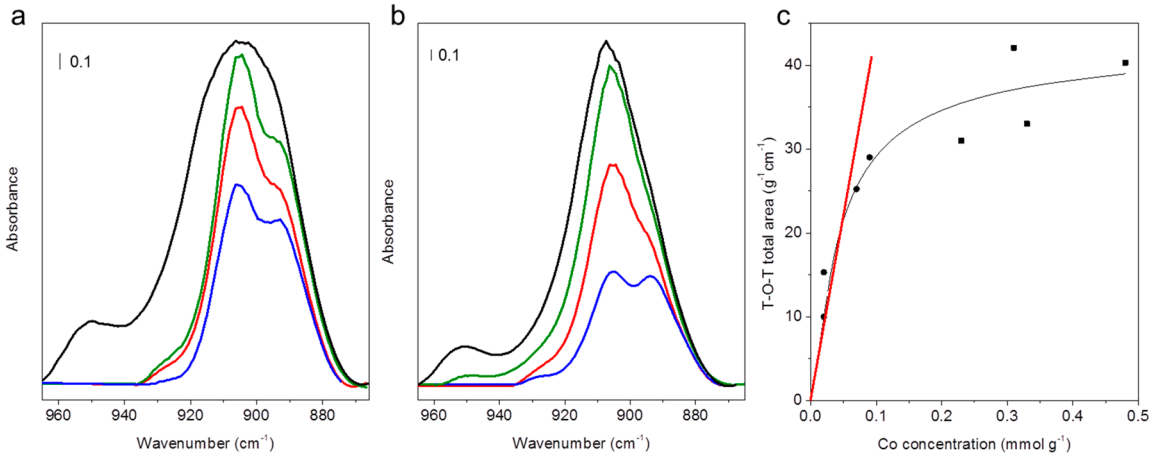

Figure 10. FTIR spectra in the region of the shifted antisymmetric T–O–T stretching lattice modes of the zeolite framework induced by binding bare Co(II) cations to the framework oxygens of dehydrated zeolites at 723 K (960–880 cm^{-1}). The Co,Na-SSZ-13 series, the samples a–d depicted in black, green, red, and blue, respectively, (a) and the Co,H-SSZ-13 series, the samples e–h depicted in black, green, red, and blue, respectively (b). The effect of the Co loading on the integrated area of vibrations for the Co,Na-SSZ-13 (■) and Co,H-SSZ-13 (●) samples (c).

DOI: 10.1021/acs.jpcc.8b07343
J. Phys. Chem. C 2019, 123, 7968–7987

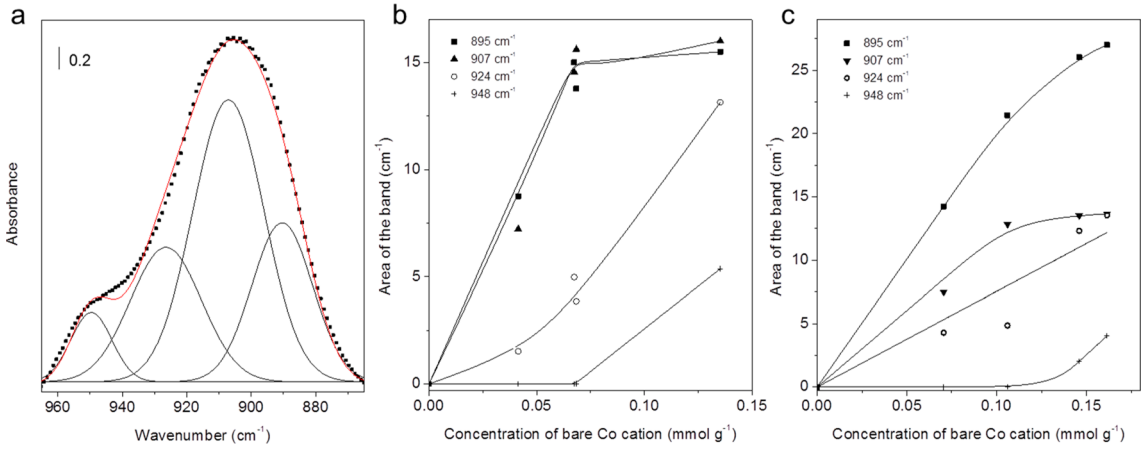

Figure 11. Simulation (●●●) of the spectra in the 960−880 cm^{-1} region in the individual Gaussian bands for the Co,H-SSZ-13 sample with the maximum Co loading (a) and the changes of the integrated area of the individual maxima at 895, 907, and 924 cm^{-1} with the concentration of Co(II) cation in the Co,Na-SSZ-13 and Co,H-SSZ-13 zeolites (b) and (c), respectively.

the shifted antisymmetric T−O−T stretching vibrations are compared with those of other zeolites in Table 5.

Table 5. Comparison of the Wavenumbers of the Shifted Antisymmetric T−O−T Stretching Vibrations of the Lattice Induced by Accommodation of Bare Co(II) Cations in the Cationic Sites

	wavenumber (cm^{-1})		wavenumber (cm^{-1})			
site	SSZ-13	site	ferrierite[57]	ZSM-5[57]	beta zeolite[39]	TNU-9[40]
σ	895	α	942−945	970	901	910
ω	907	β	918−920	931−935	918	930
τ	924	γ	905	916	935	-
τ^{3Si}	948					

The effect of the Co(II) concentration on the intensity of the individual vibrations in the Co,Na-SSZ-13 and Co,H-SSZ-13 samples is depicted in Figures 11b and 11c, respectively. As mentioned above, the concentration of the bare Co(II) cations does not increase with the rising Co cation loadings for the highest Co concentrations. This indicates the formation of another Co species than bare Co(II) cations in these samples (for details see Section 7). Therefore, the intensity of the individual bands is related to the concentration of bare Co(II) cations obtained from the total intensity of the vibrations. While the band at 924 cm^{-1} exhibits a low intensity and significantly increases at higher loadings, the bands at 895 and 907 cm^{-1} predominate in the entire range of concentrations, and the dependence of their intensity on the concentration is similar.

As mentioned above, no samples significantly differing in the relative intensity of the bands at 895 and 907 cm^{-1} were prepared. This represents an obstacle in the assignment of the

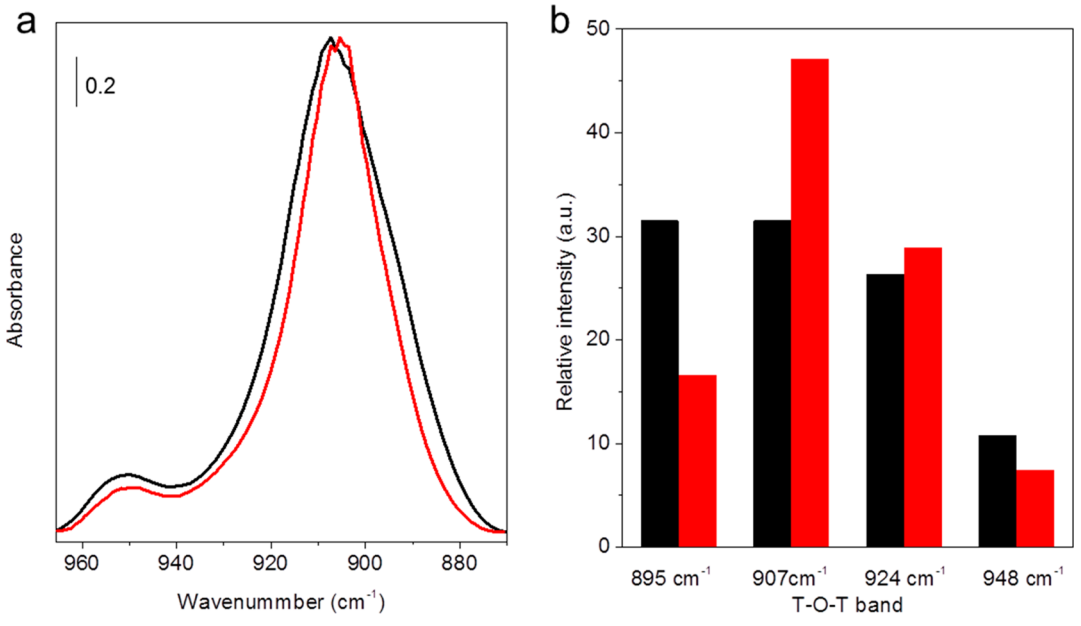

Figure 12. Differences of the vibrations in the 960−880 cm^{-1} region for the Co,H-SSZ-13 zeolite fully loaded with Co and dehydrated at 723 K (black) and the special sample (Section 2) (red), graphical representation (a), and the concentration of the simulated components (b).

DOI: 10.1021/acs.jpcc.8b07343
J. Phys. Chem. C 2019, 123, 7968−7987

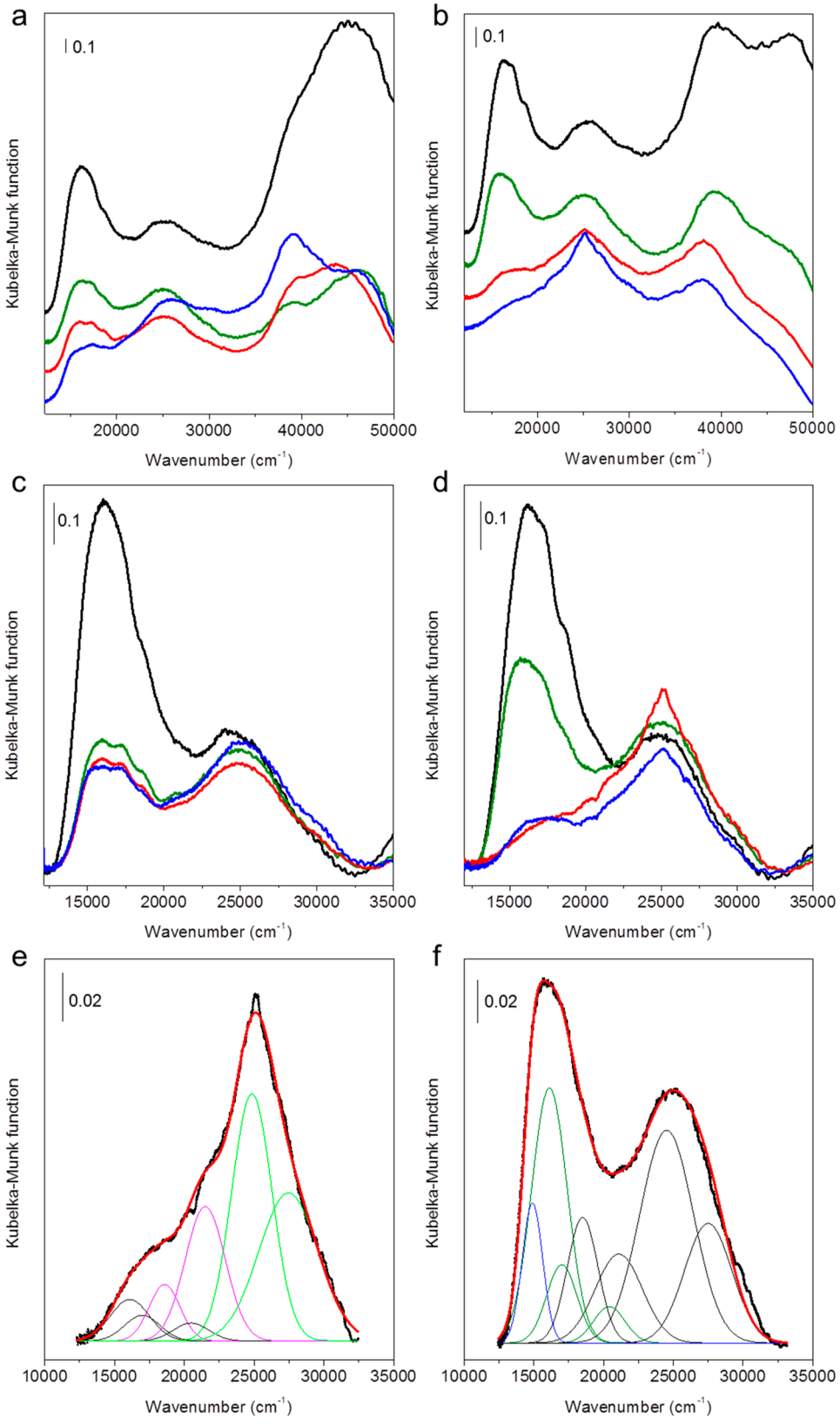

Figure 13. UV−vis spectra of the Co,Na-SSZ-13 series (a) and the Co,H-SSZ-13 series (b). All the samples were dehydrated at 723 K. Normalized vis spectra of the Co,Na-SSZ-13/a−d (black, green, red, and blue, respectively, lines) samples (c) and the Co,H-SSZ-13/e−h (black, green, red, and blue, respectively, lines) samples (d). Simulation (in red) of the vis spectra to the spectroscopic species formed by Gaussian bands of the Co,H-SSZ-13 samples with the lowest (e) and highest (f) Co loadings. The spectroscopic species in green formed by one band with the maximum at 15 000 cm^{-1} is present only for the highest Co concentrations.

DOI: 10.1021/acs.jpcc.8b07343
J. Phys. Chem. C 2019, 123, 7968−7987

Table 6. Al Distribution in the SSZ-13 Zeolite

Si/Al[a]	Al[a] mmol/g	Al_{SINGLE}[b] (% Al)	Al_{SINGLE}[b] mmol/g	Al_{CLOSE}[c] (% Al)	Al_{CLOSE}[c] mmol/g	Al_{PAIR}[d] (% Al)	Al_{PAIR}[d] mmol/g
12	1.25	35	0.44	54	0.67	11	0.14

[a]From the chemical analysis using the XRF method. [b]From the Co concentration in the zeolite maximally exchanged by Co(II) hexaaqua complex employing eq 2. [c]From the Co concentration in the zeolite maximally exchanged by Co(II) hexaaqua complex and from FTIR of adsorbed d_3-acetonitrile employing eq 4. [d]From FTIR of adsorbed d_3-acetonitrile employing eq 3.

individual bands to the cations located in the individual cationic sites (see Section 7). Therefore, an attempt was made to prepare a special sample with a significantly changed relative ratio of the bands at 895 and 907 cm^{-1} (see Section S2 of the Supporting Information for details regarding the preparation of this special sample). The FTIR spectra of this sample are compared with the spectrum of the sample prepared by the standard ion-exchange procedure in Figure 12.

Comparison indicates that while the relative intensity of the bands at 907 and 924 cm^{-1} notably and slightly, respectively, increased, the intensity of bands at 895 and 948 cm^{-1} significantly decreased.

6.6. UV−vis Spectroscopy of the Co Samples. UV−vis spectra of the dehydrated Co-SSZ-13 samples are depicted in Figures 13a and 13b.

Two types of absorption bands are present in the spectra: bands attributable to the d−d transition of bare Co(II) cations in the visible region between 12 000 and 30 000 cm^{-1} and charge transfer (CT) bands in the UV region above 40 000 cm^{-1}. The CT bands correspond to (i) charge transfer (CT) between bare Co(II) and skeletal oxygens and (ii) the Al−O and Si−O charge transfer of the zeolite framework.[39,40,55,56,58] Bands of bridging Co-oxo species with characteristic maximum at 35 000 cm^{-1} are not present in the spectra.[6,7,39] It should be noted that the CT bands of Co(II) cations are not site specific and cannot be employed for the analysis of the Co(II) siting. Therefore, our attention will be focused on the d−d spectra in the visible region.

On-sight analysis of the normalized vis spectra of the dehydrated Co samples shown in Figures 13c and 13d clearly evidences the presence of two spectroscopic species with complex bands centered at around 16 500 and 25 000 cm^{-1} and another complex spectroscopic species at around 20 000 cm^{-1}. While the spectroscopic species at 20 000 and 25 000 cm^{-1} predominate at low Co loadings, the species at 16 500 cm^{-1} prevail in the spectra of highly Co-loaded samples. The spectra were simulated using Gaussian bands for detailed analysis of the spectra (Figures 13e and 13f). The spectroscopic species at around 25 000 cm^{-1} is formed by two absorption bands at 24 500 and 27 000 cm^{-1}. Furthermore, two bands at 18 500 and 21 500 cm^{-1} belong to the species reflected in the region around 20 000 cm^{-1}. The complex spectroscopic species in the region at around 16 500 cm^{-1} is formed by three bands with the maxima at 16 100, 17 000, and 20 500 cm^{-1}. Unexpectedly, the analysis of the spectra with the highest Co loadings reveals the existence of a fourth spectroscopic species present only at the highest Co loadings. This spectroscopic species is reflected only in one band at 15 000 cm^{-1}.

7. DISCUSSION

The obtained X-ray pattern, ^{27}Al MAS NMR and ^{29}Si MAS NMR spectra, and SEM images of the Na-SSZ-13 sample showed a well-crystalline SSZ-13 zeolite with the exclusive presence of framework tetrahedral Al atoms in the zeolite (see Section 6.1). However, besides a well-developed crystal structure of the parent zeolite material, the accessibility of the whole inner volume of the zeolite channel/cavity system is also essential for the analysis of both (i) the Al distribution and (ii) the siting of divalent cations and the Al pairs forming the corresponding cationic sites. The reason is that ion-exchanged Co(II) cations acting as a probe represent the foundation of the characterization methods. 8-Rings control only the migration from the main channel to the mordenite pocket and to the side channel of ferrierite.[13] Since the maximum Me(II) ion exchange obtained for the A zeolite and chabazite is 100% (i.e., Me(II)/Al 0.5), the system of cavities interconnected by 8-rings does not represent a limitation for Co(II) cations in the SSZ-13 sample.[90−92] This is further confirmed by a complete ion exchange of our SSZ-13 sample to the NH_4-SSZ-13 form. Therefore, Co(II) cations as a probe can be employed to analyze the Al distribution and the Me(II) siting in the investigated SSZ-13 sample.

7.1. Al Distribution in the SSZ-13 Zeolite. *7.1.1. Al−O−Si−O−Al Sequences.* Our ^{29}Si MAS NMR measurements reveal that there are no Al−O−Si−O−Al sequences of Si(2Si,2Al) atoms in the investigated sample (Figure 7). Al−O−Si−O−Al sequences were reported only for Al-rich zeolites (including chabazite of the same topology as SSZ-13).

7.1.2. Single Al Atoms (Al_{SINGLE}). Single Al atoms are those which are unable to accommodate both bare Co(II) cations and Co(II) hexaaqua complexes, and their concentration is given in the case of acid catalysis by the equation

$$[Al_{SINGLE}] = [Al_{FR}] - 2x[Co_{MAX}] \quad (2)$$

where $[Co_{MAX}]$ is the Co concentration in the zeolite maximally exchanged by the Co(II) hexaaqua complex.

Our results reveal that the $[Co_{MAX}]$ value is 0.325 for the investigated SSZ-13 sample, and therefore, the single Al atoms represent 35% of the framework Al atoms in this zeolite (Table 6).

The ^{27}Al isotropic chemical shifts of 60.0 and 59.2 ppm observed in our prior study[69] correspond to the single Al atoms. This result agrees well with the fact that the ^{27}Al NMR resonance at 60.0 ppm represents ca. 25% of the Al atoms in the ^{27}Al MAS NMR and ^{27}Al 3Q MAS NMR spectra of the investigated sample.

7.1.3. Al Pairs (Al_{PAIRS}) and Close Unpaired Al Atoms (Al_{CLOSE}). Al_{PAIRS} and Al_{CLOSE} represent Al atoms of Al−O−$(Si−O)_{n\geq 2}$−Al sequences which balance Co(II) hexaaqua complexes in hydrated zeolites. Moreover, Al_{PAIRS} can accommodate bare Co(II) cations in dehydrated zeolites, while Al_{CLOSE} cannot. The concentrations of the former and latter atoms are thus given by the equations

$$[Al_{PAIR}] = 2x([Co_{BARE}] - [Co_{D6R}]) \quad (3)$$

$$[Al_{CLOSE}] = 2x[Co_{MAX}] - 2x([Co_{BARE}] - [Co_{D6R}]) \quad (4)$$

where $[Co_{BARE}]$ is the concentration of bare Co(II) cations in the maximally bare Co(II) cation exchanged zeolite; $[Co_{MAX}]$

DOI: 10.1021/acs.jpcc.8b07343
J. Phys. Chem. C 2019, 123, 7968−7987

is the Co concentration in the zeolite maximally exchanged by Co(II) hexaaqua complex; and $[Co_{D6R}]$ is the concentration of bare Co(II) cations in the hexagonal prism. It should be noted that the two Al atoms accommodating Co(II) cations in D6R exhibit ion-exchange properties of single Al atoms (do not accommodate Co(II) hexaaqua complexes in hydrated zeolites), and the acid sites in protonic forms correspond to single Al atoms as well.

7.1.4. Three Main Methods Allowing the Estimation of the Bare Co(II) Cations in Dehydrated Zeolites. Method 1. The adsorption of d_3-acetonitrile in dehydrated zeolites monitored by FTIR spectroscopy represents the simplest way to estimate the bare Co(II) cations in zeolites. The bare Co(II) cations are acceptors of lone electron pairs of the N atoms of acetonitrile, and therefore, they represent Lewis acid sites which can adsorb d_3-acetonitrile. The intensity of the IR band of d_3-acetonitrile adsorbed on bare Co(II) cations then corresponds to the concentration of the bare Co(II) cations. It should be noted that the adsorption of d_3-acetonitrile is not specific regarding the siting of the bare Co(II) cations (Al pairs) (i.e., there is only one band for all the cationic sites). The adsorption of acetonitrile on bare Co(II) cations corresponds directly to the concentration of Al pairs since acetonitrile does not adsorb on Co(II) cations accommodated in the ω cationic site inside the hexagonal prism ($[Co_{D6R}]$) since these Co(II) cations exhibit a closed coordination sphere. Nevertheless, there are substantial differences in the framework topology between pentasil ring zeolites and SSZ-13. The space for the adsorbed complex Co(II)$\cdots d_3$-acetonitrile is very limited in the case of pentasil-ring zeolites leading to different extinction coefficients of d_3-acetonitrile adsorbed on Co(II) cations in pentasil-ring zeolites and SSZ-13. Moreover, in contrast to pentasil-ring zeolites, the access to the whole zeolite cavity system of SSZ-13 occurs exclusively through 8-rings, and this can affect the applicability of the method on SSZ-13. Therefore, the adsorption of d_3-acetonitrile as a method for the analysis of bare Co(II) cations in SSZ-13 has to be verified, and the extinction coefficient has to be evaluated.

Method 2. Shifting the antisymmetric T−O−T stretching lattice modes of the zeolite framework occurred by binding bare Co(II) cations to the framework oxygens of dehydrated zeolites monitored by FTIR spectroscopy. This method is site sensitive and can be employed to distinguish the Co(II) cations accommodated in different cationic sites when the spectrum is completely analyzed. Several close bands in the FTIR spectrum of dehydrated Co-zeolites correspond to the Al pairs forming the cationic sites. Nevertheless, the extinction coefficients for Co(II) cations located in the individual sites do not differ, and the only obstacle associated with this method represents the presence of a "well-developed window" in the region of the antisymmetric T−O−T stretching lattice vibrations. The "window" is essential for observations of the vibrations reflecting the accommodated bare Co(II) cations. In addition, this method can also detect the Co(II) cations located in the ω cationic site of the hexagonal prism of SSZ-13 although the Al atoms forming this cationic site are located in two different rings.

Method 3. The absorption of bare Co(II) cations in the region of d−d transitions is monitored by vis spectroscopy. This method is also site sensitive and can be used to determine the Co(II) cations located in different cationic sites upon analyzing the vis spectrum. However, this approach is the most demanding since one or more (up to four) absorption bands in the spectrum correspond to one Co(II) coordination (i.e., cationic site). Moreover, the extinction coefficients differ for the Co(II) sites.[39,55,56,58] It should be noted that this method also includes Co(II) cations in the hexagonal prism as discussed in previous paragraphs.

7.2. Evidence of the Presence of Close Unpaired Al Atoms in the SSZ-13 Zeolite. Two close unpaired Al atoms are able to balance Co(II) hexaaqua complexes in hydrated zeolites. When the zeolite is dehydrated, the two close unpaired Al atoms cannot accommodate bare Co(II) cations. Several studies suggested that upon dehydration of the zeolite $[Co(III)O]^+$ species can be formed. They balance one Al atom of the two close unpaired Al atoms, and the other close unpaired Al atoms are balanced by a different positively charged species.[3,6,7] $[Co(III)O]^+$ species do not adsorb acetonitrile, and therefore, they cannot be monitored by FTIR spectroscopy of adsorbed d_3-acetonitrile. Moreover, $[Co(III)O]^+$ species are not "visible" in FTIR spectra in the region of the shifted antisymmetric T−O−T stretching lattice modes either.

Our results show that the intensity of d_3-acetonitrile adsorbed on bare Co(II) cations in SSZ-13 is not proportional to the Co loading in the samples (Figure 9c). The absorption linearly increases with the rising Co loading at its low values, but there is a significant deviation from the linear increase at the medium Co loading resulting in a plateau at the high Co loading. This effect is observed for both the Co,Na-SSZ-13 and Co,H-SSZ-13 samples, and therefore, it can be explained neither by a steric hindrance in the d_3-acetonitrile adsorption nor by a limited d_3-acetonitrile transport. If steric hindrance was responsible, the effect would be the strongest for the Co,Na-SSZ-13 sample with the lowest Co loading (which is not observed for our samples) since one Co(II) cation replaces two Na^+ cations (acetonitrile adsorbs on Na^+ as well). If the transport of d_3-acetonitrile was responsible, then it should be faster in Co,H-SSZ-13 than in Co,Na-SSZ-13, and the effect should not be observed for Co,H-SSZ-13 which is not true either. Therefore, the only plausible explanation of the effect is that close unpaired Al atoms are present in the SSZ-13 sample.

The presence of close unpaired Al atoms is further confirmed by the similar dependence of the intensity of the shifted antisymmetric T−O−T stretching lattice modes of the zeolite framework on the Co loading (Figure 10c). This is well visualized in Figure 14 in which the concentration of bare Co(II) cations derived from the FTIR spectra of adsorbed d_3-acetonitrile is plotted against the concentration of bare Co(II) cations obtained from the FTIR spectra of the shifted antisymmetric T−O−T vibrations.

This dependence is linear in the whole region but does not pass through zero indicating that even at low Co loadings the ω cationic site in the hexagonal prism is occupied by Co(II) cations. This fact results in systematically higher values of the concentration of bare Co(II) cations received from FTIR spectra of the shifted antisymmetric T−O−T vibrations than from the FTIR spectra of adsorbed d_3-acetonitrile.

7.3. Analysis of the Al Pairs in the SSZ-13 Zeolite. The linear parts of the concentration dependences of the FTIR spectra of the shifted antisymmetric T−O−T vibrations and the FTIR spectra of adsorbed d_3-acetonitrile can be employed to estimate the extinction coefficients for bare Co(II) cations. The values of the extinction coefficients are close to those already reported for pentasil-ring zeolites (Table 4). The knowledge of the extinction coefficients allows the estimation

DOI: 10.1021/acs.jpcc.8b07343
J. Phys. Chem. C 2019, 123, 7968−7987

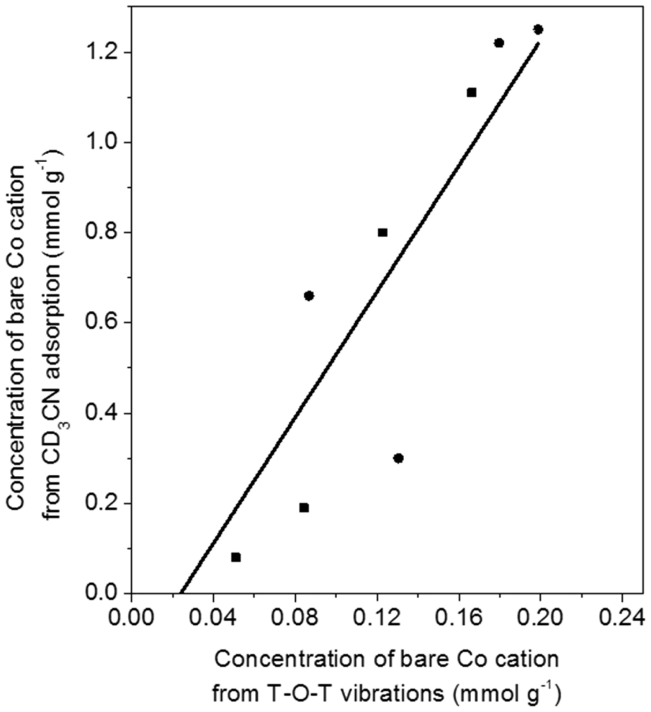

Figure 14. Intensity of the bands of d_3-acetonitrile adsorbed on bare Co(II) cations plotted against the intensity of the bands corresponding to the shifted antisymmetric T−O−T stretching vibrations. This linear dependence reaches zero for the samples containing bare Co(II) cations. This indicates that the ω site inside the hexagonal prism is occupied from the lowest Co loadings. Co,Na-SSZ-13 series (■) and Co,H-SSZ-13 series (●).

of the maximum content of bare Co(II) cations in the investigated sample. The concentration of Al pairs (Tables 6 and 7) and close unpaired Al atoms (Table 6) can be calculated employing eqs 3 and 4.

Table 7. Concentrations of Al Atoms in Al Pairs Forming the Cationic Sites in the SSZ-13 Sample

site	σ	ω	τ	τ^{3Si}
ring	6-ring	D6R	8-ring	8-ring
Me(II) sites (% of sites)	26	39	26	9
Al_{FR} (% Al)	5	7	5	2
Al (mmol/g)	0.06	0.09	0.06	0.02

It should be noted that the data in Table 7 are obtained from the FTIR spectra of the shifted antisymmetric T−O−T vibrations, and therefore, they also include the Co(II) cations in the ω site of the D6R (the Al atoms forming this site do not belong to Al pairs). Conversely, the data in Table 6 were obtained from FTIR spectra of adsorbed d_3-acetonitrile not reflecting the ω site.

Table 6 shows that the concentration of Al pairs accommodating bare Co(II) cations in the investigating SSZ-13 sample is low, reaching only 11% of all the Al atoms. 54% of all the Al atoms are present in the form of close unpaired Al atoms. Co(II) cations upon dehydration preferentially form bare divalent cations and occupy cationic sites with two Al atoms at low Co loadings. With increasing Co loadings, Co cations are exchanged to the vicinity of close unpaired Al atoms, and upon dehydration, they form $[Co(III)O]^+$ species balancing one of the two close unpaired Al atoms. At the highest Co loading, Co cations in the form of $[Co(III)O]^+$ species predominate. The corresponding close unpaired Al atoms therefore represent the most populated type of Al atoms (54%) in the framework of the SSZ-13 sample (Table 6).

To the best of our knowledge, close unpaired Al atoms have been reported only for zeolites of the *BEA topology. Their concentration reaches from 40 to 75% of Al atoms in beta zeolites with a high or medium Al content (Si/Al < 18).[3,6,7] Therefore, the SSZ-13 zeolite is the second structure with a substantial formation of these unique species of close unpaired Al atoms.

7.4. Siting of Bare Me(II) Cations, Al Pairs, and Close Unpaired Al Atoms in SSZ-13. The SSZ-13 framework is formed only by one T site.[13] However, the DFT calculations and the ^{27}Al 3Q MAS NMR experiments clearly showed the splitting of the T site into three T(Al) sites.[69] Nevertheless, the splitting does not represent a crucial issue regarding the location of the active site in the ring and cavity systems. Conversely, the siting of (i) the close unpaired Al atoms, (ii) the Al pairs forming the cationic sites, and (iii) the accommodated divalent cations is of crucial importance.

7.4.1. Siting of Close Unpaired Al Atoms (Al_{CLOSE}). $[Co(III)O]^+$ species balancing close unpaired Al atoms in dehydrated zeolites are spectroscopically "invisible" (i.e., they are not reflected in (i) FTIR spectra of the shifted antisymmetric T−O−T vibrations, (ii) FTIR spectra of adsorbed d_3-acetonitrile, and (iii) UV−vis spectra), and therefore they cannot be employed as a probe of the location of close unpaired Al atoms in the SSZ-13 cavity system. Conversely, ^{27}Al MAS NMR spectroscopy in tandem with DFT calculations of the ^{27}Al isotropic chemical shifts of these close unpaired Al atoms can be employed for this purpose.

Our ^{27}Al 3Q MAS NMR measurements yielded two ^{27}Al NMR resonances at 59.4 and 60.0 ppm. Our ^{27}Al MAS NMR experiments provided the relative concentrations which are 75% and 25%, respectively, of all the Al atoms. The ^{27}Al NMR resonance at 60.0 ppm can be assigned to single Al atoms (35% of all the Al atoms, Table 6), while that at 59.4 ppm belongs to the close unpaired Al atoms (54% of all the Al atoms, Table 6), the Al pairs forming cationic sites (11% of all the Al atoms, Table 6), and some single Al atoms. The broadening of the ^{27}Al NMR resonances at 59.4 and 60.0 ppm originates from either the variability of the middle-range and long-range orderings of the zeolite framework or the presence of other ^{27}Al NMR resonances with close NMR parameters. However, our simulations show that only ^{27}Al NMR resonances above 60.0 ppm and below 58.0 ppm can be excluded. Figure 6 shows the ^{27}Al isotropic chemical shifts calculated for the six models featuring possible locations of two close unpaired Al atoms. Comparison of the calculated and observed ^{27}Al isotropic chemical shifts clearly indicates that the structure featured in Model F is the best candidate for the siting of close unpaired Al atoms in the SSZ-13 zeolite. All the other models can be ruled out as dominant structures of close unpaired Al atoms in the SSZ-13 zeolite sample. The ^{27}Al isotropic chemical shifts of 58.6 and 59.5 ppm calculated for Model F can correspond to the observed ^{27}Al NMR resonance at 59.4 ppm.

7.4.2. Siting of Al Pairs (Al_{PAIRS}) Creating Cationic Sites for Bare Me(II) Cations. Based on XRD, three cationic sites for bare cations were suggested for zeolites of the CHA topology.[92,93] The three sites are located in (i) the hexagonal prism, (ii) the 6-ring, and (iii) the 8-ring, designated as ω, σ, and τ, respectively, as sites containing Al pairs and

DOI: 10.1021/acs.jpcc.8b07343
J. Phys. Chem. C 2019, 123, 7968−7987

accommodating bare divalent cations. However, the spectra of the shifted antisymmetric T−O−T stretching vibrations of the lattice clearly evidence four types of Co(II) coordinations, i.e., four cationic sites. Our DFT calculations of the models of the possible σ, τ, τ^{3Si}, ω, and ω^{3Si} cationic sites accommodating one Co(II) cation can explain this discrepancy.

The ω and ω^{3Si} cationic sites inside the hexagonal prism cover two possibilities with one Al atom of Al−O−$(Si-O)_2$−Al or Al−O−$(Si-O)_3$−Al sequences, respectively, in each 6-ring. The DFT calculations clearly showed that only Al−O−$(Si-O)_2$−Al sequences created a cationic site which can accommodate bare Co(II) cations which is located inside the hexagonal prism. Conversely, Al−O−$(Si-O)_3$−Al sequences do not form a cationic site which can accommodate bare Co(II) cations (for details see Section 5.1.). Therefore, it is safe to conclude that the ω site of bare divalent cations inside the D6R is formed by an Al−O−$(Si-O)_2$−Al sequence with each Al atom in one 6-ring of the hexagonal prism. The calculated ^{27}Al isotropic chemical shifts of the Al atoms creating this site are 58.6 and 59.2 ppm (Figure 4). Bare Co(II) cations in this site exhibit approximately pseudo-octahedral coordination with the coordination to three framework oxygens with the access strictly limited by the 6-ring.

There is only one possible arrangement of the σ site of the 6-ring with two Al atoms in Al−O−$(Si-O)_2$−Al pairs. The calculated ^{27}Al isotropic chemical shifts of the Al atoms forming this site are 57.4 and 58.2 ppm (Figure 4), corresponding to this site. Co(II) cations in this site exhibit approximately square planar coordination in the plane of the 6-ring and are coordinated to four oxygens of this ring.

The τ and τ^{3Si} cationic sites in the 8-ring can be created by Al−O−$(Si-O)_2$−Al and Al−O−$(Si-O)_3$−Al, respectively, pairs. Our DFT calculations revealed that both the pairs can form a cationic site which can accommodate bare Co(II) cations located inside the 8-ring. Therefore, there are two types of cationic sites in the 8-ring: τ and τ^{3Si}. The computed ^{27}Al isotropic chemical shifts of the Al atoms forming these cationic sites are 58.6 and 59.3 ppm (Al−O−$(Si-O)_2$−Al) and 56.7 and 57.3 ppm (Al−O−$(Si-O)_3$−Al) (Figure 5). Co(II) cations in this site exhibit a highly open coordination sphere with coordination to three oxygen atoms of the 8-ring in the plane of the ring. The τ^{3Si} site represents the first cationic sites created by an Al pair with the Al atoms separated by three Si atoms.

In opposition to close unpaired Al atoms, ^{27}Al MAS NMR and ^{27}Al 3Q MAS NMR experiments combined with DFT calculations of the ^{27}Al isotropic chemical shifts of the Al atoms of the Al pairs (Figures 4 and 5) cannot be employed for the analysis of the Al pairs. Table 7 shows that the maximum concentration of one Al atom of the Al pair forming the cationic sites does not exceed 4% of all the Al atoms. This low Al concentration is at the edge of the experimental limit of the ^{27}Al MAS NMR experiment. However, in contrast to close unpaired Al atoms, bare Co(II) cations balanced by Al pairs can be easily detected by FTIR spectroscopy and vis spectroscopy, and they can serve as probes for the location of Al pairs.

7.5. Siting of Bare Me(II) Cations. Figure 11 clearly shows four bands with their maxima at 895, 907, 924, and 948 cm^{-1} corresponding to four types of bare Co(II) cations in the cationic sites of SSZ-13. The concentration of Co(II) cations in the individual sites of the samples is depicted in Figure 11a. Because a significant fraction of the Co(II) cations balances close unpaired Al atoms, the effect of the Co loading on the shifted antisymmetric T−O−T stretching vibrations of the lattice induced by binding bare Co(II) cations to the framework oxygens does not provide good insight into the occupation of cationic sites. The concentration of Co(II) cations in the individual sites is plotted against the concentration of bare Co(II) cations in the samples in Figures 11b and 11c. It should be pointed out that the shifted antisymmetric T−O−T stretching vibrations corresponding to the siting of Co(II) cations in SSZ-13 and pentasil-ring zeolites differ (Table 5) due to different geometries of the cationic sites in SSZ-13 (and in materials of the CHA topology in general) and pentasil-ring zeolites. This difference is responsible for the fact that the wavenumbers of the vibrations cannot be simply assigned to the cationic sites of the SSZ-13 zeolite as was possible for the pentasil-ring TNU-9 zeolite.[40] Therefore, the assignment of the vibrations to the Co(II) cations in the individual cationic sites requires a detailed discussion.

Conversely, Co(II) d−d transitions are highly sensitive to the local environment and reflect the arrangement of the cationic sites, and therefore, Co(II) monitored by vis spectroscopy can serve as a probe of the siting of Co(II) and the corresponding Al pairs. Nevertheless, the individual Co(II) spectroscopic species can be interpreted only semi-empirically (based on the similarity of the sites and spectra in various zeolites) due to the fact that even state of the art quantum chemistry methods do not allow the prediction of the absorption spectrum of Co(II) cation exchanged in zeolite matrices with a high enough accuracy. Spectra of bare Co(II) cations in different cationic sites of various zeolites are listed in Table S3 of the Supporting Information to help interprete the vis spectra of the SSZ-13 zeolite (Figure 13).

It should be mentioned that the detailed quantitative analysis of the Co(II) vis spectra is extremely demanding and, in some circumstances, even extremely difficult. Moreover, the extinction coefficients of Co(II) cations in the individual sites can significantly differ. Therefore, the most promising approach for the analysis of the Co(II) siting is a combination of vis spectroscopy for the identification of the arrangements of the cationic sites and FTIR spectroscopy of the shifted antisymmetric T−O−T vibrations for quantitative analysis of the distribution of Co(II) cations in the individual sites. The quantitative results of the analysis of Co and Al pair distribution are shown in Table 7.

7.5.1. ω Cationic Site. This site corresponds to the band at 907 cm^{-1}. It is preferentially occupied from low loadings in both the Co,H-SSZ-13 and Co,Na-SSZ-13 samples, and the concentration of Co(II) cations in this site steadily increases with the Co loading. This site accommodates 39% of the bare Co(II) cations and 7% of the framework Al atoms in the maximally Co-loaded zeolite (Table 7). The occupancy of the sites corresponding to the vibrations at 895 and 907 cm^{-1} from the lowest Co loadings indicates that one of them represents the ω site inside the hexagonal prism. The dependence shown in Figure 14 is linear in the whole region but does not pass through zero indicating that even at low Co loadings the ω cationic site in the hexagonal prism is occupied by Co(II) cations. The significant increase of the relative intensity of the band at 907 cm^{-1} in the special sample (see Section S2 of the Supporting Information for details regarding the preparation of this special sample) clearly evidences that this band corresponds to the Co(II) cation in the ω site. This site is

DOI: 10.1021/acs.jpcc.8b07343
J. Phys. Chem. C 2019, 123, 7968−7987

accessible only through the 6-ring, and thus, in contrast to all the other sites, a release of a Co(II) cation from this site and its replacement by a Na^+ cation are strictly limited. The preferential occupation of the ω site agrees well with the fact that the Co(II) cation binds the second most tightly in this site (after the σ site) (Table 2).

The doublet centered around 20 000 cm^{-1} can be attributed to the Co(II) cation in the octahedral or pseudo-octahedral symmetry (Table S3 of the Supporting Information). Co(II) cations with the pseudo-octahedral coordination and similar spectrum were reported for hexagonal prism of the zeolite Y.[94,95] The exact coordination of divalent cations in this site of the above zeolite is not known, but the hexagonal prism of the zeolite Y is very similar to that of SSZ-13. Therefore, the doublet around 20 000 cm^{-1} reflects the Co(II) cations located in the ω site of the hexagonal prism.

7.5.2. σ Cationic Site. The doublet centered around 25 000 cm^{-1} can be without any doubt assigned to the Co(II) cation located in the σ site. This assignment is based on the comparison with the spectra of the Co-A zeolite, for which the doublet around 25 000 cm^{-1} was attributed by Klier et al. to the Co(II) cation in the planar C_{3v} symmetry in the plane of the simple 6-ring (Table S3 of the Supporting Information).[96,97] Therefore, Co(II) cations located in the plane of the 6-ring of the hexagonal prism were assigned to the σ site. It should be noted that such doublets are not observed for the Co−Y zeolite which also contains hexagonal prisms with 6-ring.[94,95] However, in the case of the zeolite Y, a high framework Al content results in the occupation of both the opposite 6-rings of one D6R by cations with their position located significantly above the plane of the 6-ring and so with the loss of the planar symmetry. The occupation of only one 6-ring of D6R by an Al pair is assumed for the SSZ-13 sample with a low content of framework Al atoms (Si/Al 12). It should be noted that the interaction of Co(II) cation in this ring with a Na^+ cation in the opposite ring can be excluded because a formation of D6R with three Al atoms is not very probable due to the low Al content. Klier et al. showed[96,97] that the doublet at 25 000 cm^{-1} corresponds to Co(II) cations in regular 6-rings with the coordination exhibiting the trigonal planar symmetry, while our DFT calculations yielded the structure with the Co(II) cation in the 6-ring of SSZ-13 having approximately square planar symmetry (Figure 3). This can be explained by the fact that the exact symmetry of the cations in the Co-A zeolite is not known, and XRD studies showed that Co(II) cations are located in the center of the 6-ring. Conversely, the structure depicted in Figure 3 depicts beside the location in the center of the ring also the ring deformation due to the coordination of the Co(II) cation to the oxygens belonging to two AlO_4^- tetrahedra. Nevertheless, the planarity and a high degree of symmetry of the site are preserved. It should be noted that due to the high symmetry of this site resulting in symmetry-forbidden d−d transitions even a weak intensity of this doublet can represent a significant part of bare Co(II) cations in the zeolite.

This site is preferentially occupied in both the Co,H-SSZ-13 and Co,Na-SSZ-13 zeolites, and from middle Co loadings, the site is saturated. This site accommodates 26% of the bare Co(II) cations and 5% of the framework Al atoms in the maximally Co-loaded zeolite (Table 7). The preferential occupation of the σ site agrees well with the fact that the Co(II) cation binds the most tightly in this site (Table 2). The band at 895 cm^{-1} can be assigned to the σ site since it reflects the cationic site which is occupied preferentially from low loadings in both the Co,H-SSZ-13 and Co,Na-SSZ-13 samples, and then it reaches a plateau approximately before one-half of bare Co(II) cations are introduced in the zeolite.

7.5.3. τ Cationic Site. The complex absorption centered at around 16 500 cm^{-1} composed of three bands can be attributed to the Co(II) cations located in the τ site of the 8-ring. This agrees well with the fact that such absorption species were not reported for pentasil-ring zeolites (they exhibit a significantly broader quartet in this region reflecting Co(II) cations in deformed 6-rings)[39,40,55,56,58] which do not exhibit cationic sites formed by the planar 8-ring. Conversely, a similar absorption was reported for the zeolite A which besides cations located in the 6-ring also exhibit cations located in the planar 8-ring of a similar shape as that in SSZ-13.[96,97] It should be noted that this triplet cannot represent a tetrahedrally coordinated Co(II) cation (only Co(II) coordinated to three framework oxygens with some adsorbed molecule, e.g., water, would be possible in zeolites)[96,97] due to the fact that this triplet is present only in the vis region of the spectra and not in the NIR one (the NIR spectrum of the dehydrated Co samples is not shown). The presence of triplets with the same splitting both at around 17 000 cm^{-1} in the vis and at around 7000 cm^{-1} in NIR regions is typical for tetrahedral coordination of the Co(II) cation in zeolites. The τ site is not significantly occupied at low Co loadings (it is more populated in the Co,Na-SSZ-13 sample than in the Co,H-SSZ-13 one), but its relative occupation significantly increases with the rising Co loading. This agrees well with the fact that the Co(II) cation binds only the third most tightly in this site (after the σ and ω sites) (Table 2). The band at 924 cm^{-1} can be assigned to the τ site. This site accommodates 26% of the bare Co(II) cations and 5% of the framework Al atoms in the maximally Co-loaded zeolite (Table 7).

7.5.4. τ^{3Si} Cationic Site. Finally, the single band at 14 500 cm^{-1} is detectable only at highest Co loadings and corresponds therefore to the FTIR band at 948 cm^{-1} which is also present only at elevated Co loadings. The τ^{3Si} cationic site corresponds to these bands. The Co(II) cation binds the least tightly in this site (Table 2). Only 9% of the bare Co(II) cations balance the Al atoms (2% of all the Al atoms) of the Al pair which creates this cationic site.

8. CONCLUSIONS

The Al distribution in the SSZ-13 zeolite with Si/Al 12 was determined, and furthermore, the siting of (i) the Al pairs forming the sites for bare divalent cations and (ii) close unpaired Al atoms were determined. Divalent cationic species can be accommodated by both Al−O−$(Si−O)_2$−Al and Al−O−$(Si−O)_3$−Al sequences in the SSZ-13 zeolite. Therefore, a new significantly improved procedure for the analysis of the arrangements of Al−O−$(Si−O)_2$−Al and Al−O−$(Si−O)_3$−Al sequences was developed. It includes in addition to the standard methods based on Co(II) cations as probes monitored by FTIR spectroscopy and UV−vis spectroscopy also ^{27}Al 3Q MAS NMR spectroscopy and extensive periodic DFT calculations including molecular dynamics. This multi-spectroscopic and theoretical approach was shown to be a very powerful tool for analyzing the organization of Al and siting of divalent cations in the SSZ-13 zeolite.

Our results reveal that 54% of all the Al atoms in the SSZ-13 zeolite are close unpaired Al atoms of Al−O−$(Si−O)_3$−Al sequences of two D6R cages with one Al located in the 4-ring

DOI: 10.1021/acs.jpcc.8b07343
J. Phys. Chem. C 2019, 123, 7968−7987

connecting two D6R units. 35% and 11% of all the Al atoms represent single Al atoms and Al pairs, respectively. The latter correspond to Al−O−(Si−O)$_{2,3}$−Al sequences located in one ring forming cationic sites for bare divalent cations. The Al atoms of Al−O−(Si−O)$_2$−Al sequences in D6R (each Al in one 6-ring) represent 7% of all the Al atoms, but the acid sites connected with these Al atoms face different cavities and, therefore, exhibit the properties typical for isolated acid sites. Divalent cations accommodated in these sites are not accessible for guest molecules. The concentration of Al−O−Si−O−Al sequences in the SSZ-13 sample is negligible.

All the types of the Al arrangements−single Al atoms, close unpaired Al atoms, and Al pairs are important for the catalytic properties of the prepared materials. Single Al atoms are able to accommodate exclusively monovalent cationic species, while Al pairs can stabilize divalent cations and divalent species. In addition, Al pairs can also create two close and cooperating monovalent centers. Close unpaired Al atoms have been until now regarded to be unique for beta zeolites with a high or medium Al content in the framework. They were reported to be responsible for the formation of monovalent oxo-species of divalent cations. The concentrations of single Al atoms, close unpaired Al atoms, and Al pairs in the SSZ-13 zeolite are the most similar to those of some Al-rich beta zeolites.

There are four cationic sites in the SSZ-13 zeolite capable of accommodating bare divalent cations. The σ site is formed by an Al−O−(Si−O)$_2$−Al sequence in the 6-ring. The divalent cation in this site exhibits planar coordination with an open coordination sphere and is coordinated to four framework oxygens of two AlO_4^- tetrahedra. This site represents the main cationic sites for accessible divalent cations which accommodates 26% of bare divalent cations in the maximum Me(II)-loaded zeolite, and the Al atoms in the Al pairs of this site correspond to 5% of all the Al atoms in the SSZ-13 zeolite. This site is preferentially occupied from the lowest cation loadings.

The τ and τ^{3Si} sites are formed by Al−O−(Si−O)$_2$−Al and Al−O−(Si−O)$_3$−Al, respectively, sequences in the 8-ring. Divalent cations located in these sites exhibit an open coordination sphere and approximately planar coordination. They are coordinated to three framework oxygens. The τ and τ^{3Si} sites accommodate 26 and 9%, respectively, of bare divalent cations in the maximum Me(II)-loaded zeolite, and the Al atoms of the Al pairs of these sites correspond to 5 and 2%, respectively, of all the Al atoms in the SSZ-13 zeolite. These sites are occupied only at higher or the highest Me(II) loadings, respectively, in the SSZ-13 zeolite.

The ω site is located inside the D6R unit. It is formed by an Al−O−(Si−O)$_2$−Al sequence with each Al atom belonging to a different 6-ring of the D6R cage. Divalent cations located in this site are coordinated to three oxygens, to one from each of the two AlO_4^- tetrahedra, and to one from a SiO_4 tetrahedron. Divalent cations in this site are not accessible for guest molecules, and the acid sites corresponding to the two Al atoms of this site face different cavities and behave as isolated acid sites. The ω site accommodates 39% of bare divalent cations in the maximum Me(II)-loaded zeolite, and the Al atoms of the Al pairs of this site correspond to 7% of all the Al atoms in the SSZ-13 zeolite.

■ ASSOCIATED CONTENT

Supporting Information

The Supporting Information is available free of charge on the ACS Publications website at DOI: 10.1021/acs.jpcc.8b07343.

XRD pattern of the calcined SSZ-13 sample (Figure S1). SEM images of the calcined SSZ-13 sample (Figure S2). ^{27}Al NMR shieldings and ^{27}Al isotropic chemical shifts calculated for the models of the cationic sites (Table S1). ^{27}Al NMR shieldings and ^{27}Al isotropic chemical shifts calculated for the models of the of Al_{CLOSE} atoms (Table S2). Section S2. Experimental. Section S4. Computational models and methods. Comparison of the spectra of Co(II) cations in the individual sites of SSZ-13 and in selected zeolites (Table S3). (PDF)

■ AUTHOR INFORMATION

Corresponding Author

*E-mail: stepan.sklenak@jh-inst.cas.cz. Tel.: (+420) 266 053 607.

ORCID

Robert Karcz: 0000-0001-9780-8214
Petr Sazama: 0000-0001-7795-2681
Stepan Sklenak: 0000-0003-4862-857X

Notes

The authors declare no competing financial interest.

■ ACKNOWLEDGMENTS

This work was supported by the Grant Agency of the Czech Republic under projects: # 17-00742S and 15-14007S and the RVO: 61388955. For zeolite synthesis, the authors acknowledge the assistance provided by the Research Infrastructure NanoEnviCz, supported by the Ministry of Education, Youth and Sports of the Czech Republic under Project No. LM2015073. The DFT calculations were supported by The Ministry of Education, Youth, and Sports from the Large Infrastructures for Research, Experimental Development and Innovations project, "IT4Innovations National Science Center − LM2015070". Chemical analyses of samples were provided in the frame of CATPRO (Ministry of Education, Youth and Sports, ref. no. MSMT-1000/2016, under Project No. LM2015039), which has been integrated into the National Programme for Sustainability I of the Ministry of Education, Youth and Sports of the Czech Republic through the project Development of the UniCRE Centre, Project Code LO1606.

■ REFERENCES

(1) Dedecek, J.; Sobalik, Z.; Wichterlova, B. Siting and Distribution of Framework Aluminium Atoms in Silicon-Rich Zeolites and Impact on Catalysis. *Catal. Rev.: Sci. Eng.* **2012**, *54*, 135−223.

(2) Sklenak, S.; Andrikopoulos, P. C.; Whittleton, S. R.; Jirglova, H.; Sazama, P.; Benco, L.; Bucko, T.; Hafner, J.; Sobalik, Z. Effect of the Al Siting on the Structure of Co(II) and Cu(II) Cationic Sites in Ferrierite. A Periodic DFT Molecular Dynamics and FTIR Study. *J. Phys. Chem. C* **2013**, *117*, 3958−3968.

(3) Sazama, P.; Tabor, E.; Klein, P.; Wichterlova, B.; Sklenak, S.; Mokrzycki, L.; Pashkkova, V.; Ogura, M.; Dedecek, J. Al-Rich Beta Zeolites. Distribution of Al Atoms in the Framework and Related Protonic and Metal-Ion Species. *J. Catal.* **2016**, *333*, 102−114.

(4) Dedecek, J.; Wichterlova, B. Geometry of the Cu^+ 540 nm Luminescence Centres in Zeolites. *Phys. Chem. Chem. Phys.* **1999**, *1*, 629−637.

DOI: 10.1021/acs.jpcc.8b07343
J. Phys. Chem. C 2019, 123, 7968−7987

(5) Dedecek, J.; Capek, L.; Wichterlova, B. Nature of Active Sites in Decane-SCR-NO_X and NO Decomposition over Cu-ZSM-5 Zeolites. *Appl. Catal., A* **2006**, *307*, 156−164.
(6) Capek, L.; Dedecek, J.; Wichterlova, B. Co-Beta Zeolite Highly Active in Propane-SCR-NO_x in the Presence of Water Vapor: Effect of Zeolite Preparation and Al Distribution in the Framework. *J. Catal.* **2004**, *227*, 352−366.
(7) Capek, L.; Dedecek, J.; Sazama, P.; Wichterlova, B. The Decisive Role of the Distribution of Al in the Framework of Beta Zeolites on the Structure and Activity of Co Ion Species in Propane-SCR-NO_x in the Presence of Water Vapour. *J. Catal.* **2010**, *272*, 44−54.
(8) Sklenak, S.; Andrikopoulos, P. C.; Boekfa, B.; Jansang, B.; Novakova, J.; Benco, L.; Bucko, T.; Hafner, J.; Dedecek, J.; Sobalik, Z. N_2O Decomposition over Fe-Zeolites: Structure of the Active Sites and the Origin of the Distinct Reactivity of Fe-Ferrierite, Fe-ZSM-5, and Fe-Beta. A Combined Periodic DFT and Multispectral Study. *J. Catal.* **2010**, *272*, 262−274.
(9) Sobalik, Z.; Sazama, P.; Dedecek, J.; Wichterlova, B. Critical Evaluation of the Role of the Distribution of Al Atoms in the Framework for the Activity of Metallo-Zeolites in Redox N_2O/NO_x Reactions. *Appl. Catal., A* **2014**, *474*, 178−185.
(10) Sazama, P.; Wichterlova, B.; Sklenak, S.; Parvulescu, V. I.; Candu, N.; Sadovska, G.; Dedecek, J.; Klein, P.; Pashkova, V.; Stastny, P. Acid and Redox Activity of Template-Free Al-Rich H-BEA* and Fe-BEA* Zeolites. *J. Catal.* **2014**, *318*, 22−33.
(11) Liang, T. Y.; Chen, J. L.; Qin, Z. F.; Li, J. F.; Wang, P. F.; Wang, S.; Wang, G. F.; Dong, M.; Fan, W. B.; Wang, J. G. Conversion of Methanol to Olefins over H-ZSM-5 Zeolite: Reaction Pathway Is Related to the Framework Aluminum Siting. *ACS Catal.* **2016**, *6*, 7311−7325.
(12) http://www.iza-structure.org/IZA-SC/framework.php?STC=CHA (accessed October 25, 2018).
(13) Database of Zeolite Structures. http://www.iza-structure.org/databases (accessed October 25, 2018).
(14) Barthomeuf, D. Topology and Maximum Content of Isolated Species (Al, Ga, Fe, B, Si,···) in a Zeolitic Framework - an Approach to Acid Catalysis. *J. Phys. Chem.* **1993**, *97*, 10092−10096.
(15) Zones, S. I. U.S. Patent US4 544 538, 1985.
(16) Andersen, J.; Bailie, J. E.; Casci, J. L.; Chen, H. Y.; Fedeyko, J. M.; Foo, R. K. S.; Rajaram, R. R. International Patent WO/2008/132452, 2008.
(17) Kwak, J. H.; Tonkyn, R. G.; Kim, D. H.; Szanyi, J.; Peden, C. H. F. Excellent Activity and Selectivity of Cu-SSZ-13 in the Selective Catalytic Reduction of NO_x with NH_3. *J. Catal.* **2010**, *275*, 187−190.
(18) Deka, U.; Juhin, A.; Eilertsen, E. A.; Emerich, H.; Green, M. A.; Korhonen, S. T.; Weckhuysen, B. M.; Beale, A. M. Confirmation of Isolated Cu^{2+} Ions in SSZ-13 Zeolite as Active Sites in NH_3-Selective Catalytic Reduction. *J. Phys. Chem. C* **2012**, *116*, 4809−4818.
(19) Gao, F.; Kwak, J. H.; Szanyi, J.; Peden, C. H. F. Current Understanding of Cu-Exchanged Chabazite Molecular Sieves for Use as Commercial Diesel Engine $DeNO_X$ Catalysts. *Top. Catal.* **2013**, *56*, 1441−1459.
(20) Szanyi, J.; Yi, C. W.; Mudiyanselage, K.; Kwak, J. H. Understanding Automotive Exhaust Catalysts Using a Surface Science Approach: Model NO_x Storage Materials. *Top. Catal.* **2013**, *56*, 1420−1440.
(21) Liu, Z.; Wakihara, T.; Oshima, K.; Nishioka, D.; Hotta, Y.; Elangovan, S. P.; Yanaba, Y.; Yoshikawa, T.; Chaikittisilp, W.; Matsuo, T.; et al. Widening Synthesis Bottlenecks: Realization of Ultrafast and Continuous-Flow Synthesis of High-Silica Zeolite SSZ-13 for NO_x Removal. *Angew. Chem., Int. Ed.* **2015**, *54*, 5683−5687.
(22) Martin, N.; Moliner, M.; Corma, A. High Yield Synthesis of High-Silica Chabazite by Combining the Role of Zeolite Precursors and Tetraethylammonium: SCR of NO_x. *Chem. Commun.* **2015**, *51*, 9965−9968.
(23) Xu, R.; Zhang, R.; Liu, N.; Chen, B.; Qiao, S. Z. Template Design and Economical Strategy for the Synthesis of SSZ-13 (CHA-Type) Zeolite as an Excellent Catalyst for the Selective Catalytic Reduction of NO_x by Ammonia. *ChemCatChem* **2015**, *7*, 3842−3847.
(24) Olsbye, U.; Svelle, S.; Bjorgen, M.; Beato, P.; Janssens, T. V. W.; Joensen, F.; Bordiga, S.; Lillerud, K. P. Conversion of Methanol to Hydrocarbons: How Zeolite Cavity and Pore Size Controls Product Selectivity. *Angew. Chem., Int. Ed.* **2012**, *51*, 5810−5831.
(25) Deimund, M. A.; Harrison, L.; Lunn, J. D.; Liu, Y.; Malek, A.; Shayib, R.; Davis, M. E. Effect of Heteroatom Concentration in SSZ-13 on the Methanol-to-Olefins Reaction. *ACS Catal.* **2016**, *6*, 542−550.
(26) Li, Z.; Navarro, M. T.; Martinez-Triguero, J.; Yu, J.; Corma, A. Synthesis of Nano-SSZ-13 and its Application in the Reaction of Methanol to Olefins. *Catal. Sci. Technol.* **2016**, *6*, 5856−5863.
(27) Dai, W.; Sun, X.; Tang, B.; Wu, G.; Li, L.; Guan, N.; Hunger, M. Verifying the Mechanism of the Ethene-to-Propene Conversion on Zeolite H-SSZ-13. *J. Catal.* **2014**, *314*, 10−20.
(28) Hudson, M. R.; Queen, W. L.; Mason, J. A.; Fickel, D. W.; Lobo, R. F.; Brown, C. M. Unconventional, Highly Selective CO_2 Adsorption in Zeolite SSZ-13. *J. Am. Chem. Soc.* **2012**, *134*, 1970−1973.
(29) Zhao, Z.; Yu, R.; Zhao, R.; Shi, C.; Gies, H.; Xiao, F. S.; De Vos, D.; Yokoi, T.; Bao, X.; Kolb, U.; et al. Cu-Exchanged Al-Rich SSZ-13 Zeolite from Organotemplate-Free Synthesis as NH_3-SCR Catalyst: Effects of Na^+ Ions on the Activity and Hydrothermal Stability. *Appl. Catal., B* **2017**, *217*, 421−428.
(30) Song, J.; Wang, Y.; Walter, E. D.; Washton, N. M.; Mei, D.; Kovarik, L.; Engelhard, M. H.; Prodinger, S.; Wang, Y.; Peden, C. H. F.; et al. Toward Rational Design of Cu/SSZ-13 Selective Catalytic Reduction Catalysts: Implications from Atomic-Level Understanding of Hydrothermal Stability. *ACS Catal.* **2017**, *7*, 8214−8227.
(31) Dusselier, M.; Davis, M. E. Small-Pore Zeolites: Synthesis and Catalysis. *Chem. Rev.* **2018**, *118*, 5265−5329.
(32) Zhao, Z.; Xing, Y.; Li, S.; Meng, X.; Xiao, F. S.; McGuire, R.; Parvulescu, A. N.; Mueller, U.; Zhang, W. Mapping Al Distributions in SSZ-13 Zeolites from ^{23}Na Solid-State NMR Spectroscopy and DFT Calculations. *J. Phys. Chem. C* **2018**, *122*, 9973−9979.
(33) Perea, D. E.; Arslan, I.; Liu, J.; Ristanovic, Z.; Kovarik, L.; Arey, B. W.; Lercher, J. A.; Bare, S. R.; Weckhuysen, B. M. Determining the Location and Nearest Neighbours of Aluminium in Zeolites with Atom Probe Tomography. *Nat. Commun.* **2015**, *6*, 7589.
(34) Di Iorio, J. R.; Gounder, R. Controlling the Isolation and Pairing of Aluminum in Chabazite Zeolites Using Mixtures of Organic and Inorganic Structure-Directing Agents. *Chem. Mater.* **2016**, *28*, 2236−2247.
(35) Di Iorio, J. R.; Nimlos, C. T.; Gounder, R. Introducing Catalytic Diversity into Single-Site Chabazite Zeolites of Fixed Composition via Synthetic Control of Active Site Proximity. *ACS Catal.* **2017**, *7*, 6663−6674.
(36) Dedecek, J.; Kaucky, D.; Wichterlova, B. Al Distribution in ZSM-5 Zeolites: An Experimental Study. *Chem. Commun.* **2001**, 970−971.
(37) Dedecek, J.; Kaucky, D.; Wichterlova, B.; Gonsiorova, O. Co^{2+} Ions as Probes of Al Distribution in the Framework of Zeolites. ZSM-5 Study. *Phys. Chem. Chem. Phys.* **2002**, *4*, 5406−5413.
(38) Dedecek, J.; Lucero, M. J.; Li, C. B.; Gao, F.; Klein, P.; Urbanova, M.; Tvaruzkova, Z.; Sazama, P.; Sklenak, S. Complex Analysis of the Aluminum Siting in the Framework of Silicon-Rich Zeolites. A Case Study on Ferrierites. *J. Phys. Chem. C* **2011**, *115*, 11056−11064.
(39) Dedecek, J.; Capek, L.; Kaucky, D.; Sobalik, Z.; Wichterlova, B. Siting and Distribution of the Co Ions in Beta Zeolite: A UV-vis-NIR and FTIR Study. *J. Catal.* **2002**, *211*, 198−207.
(40) Karcz, R.; Dedecek, J.; Supronowicz, B.; Thomas, H. M.; Klein, P.; Tabor, E.; Sazama, P.; Pashkova, V.; Sklenak, S. TNU-9 Zeolite: Aluminum Distribution and Extra-Framework Sites of Divalent Cations. *Chem. - Eur. J.* **2017**, *23*, 8857−8870.
(41) Sklenak, S.; Dedecek, J.; Li, C. B.; Wichterlova, B.; Gabova, V.; Sierka, M.; Sauer, J. Aluminum Siting in Silicon-Rich Zeolite Frameworks: A Combined High-Resolution ^{27}Al NMR Spectroscopy and Quantum Mechanics/Molecular Mechanics Study of ZSM-5. *Angew. Chem., Int. Ed.* **2007**, *46*, 7286−7289.

DOI: 10.1021/acs.jpcc.8b07343
J. Phys. Chem. C 2019, 123, 7968−7987

(42) Sklenak, S.; Dedecek, J.; Li, C.; Wichterlova, B.; Gabova, V.; Sierka, M.; Sauer, J. Aluminium Siting in the ZSM-5 Framework by Combination of High Resolution ^{27}Al NMR and DFT/MM Calculations. *Phys. Chem. Chem. Phys.* **2009**, *11*, 1237−1247.
(43) Gaertner, C. A.; van Veen, A. C.; Lercher, J. A. Oxidative Dehydrogenation of Ethane on Dynamically Rearranging Supported Chloride Catalysts. *J. Am. Chem. Soc.* **2014**, *136*, 12691−12701.
(44) Fickel, D. W.; Fedeyko, J. M.; Lobo, R. F. Copper Coordination in Cu-SSZ-13 and Cu-SSZ-16 Investigated by Variable-Temperature XRD. *J. Phys. Chem. C* **2010**, *114*, 1633−1640.
(45) Broussard, L.; Shoemaker, D. P. The Structures of Synthetic Molecular Sieves. *J. Am. Chem. Soc.* **1960**, *82*, 1041−1051.
(46) Smith, J. V. Crystal Structures with a Chabazite Framework. I. Dehydrated Ca-Chabazite. *Acta Crystallogr.* **1962**, *15*, 835−845.
(47) Eulenberger, G. R.; Shoemaker, D. P.; Keil, J. G. Crystal Structures of Hydrated and Dehydrated Synthetic Zeolites with Faujasite Aluminosilicate Frameworks. I. Dehydrated Sodium Potassium and Silver Forms. *J. Phys. Chem.* **1967**, *71*, 1812−1819.
(48) Mortier, W. J. *Extraframework Cationic Positions in Zeolites*; Elsewier: Amsterdam, 1982.
(49) Engelhardt, G.; Lohse, U.; Lippmaa, E.; Tarmak, M.; Magi, M. ^{29}Si NMR Investigation of Silicon-Aluminum Ordering in the Aluminosilicate Framework of Faujasite-Type Zeolites. *Z. Anorg. Allg. Chem.* **1981**, *482*, 49−64.
(50) Klinowski, J.; Ramdas, S.; Thomas, J. M.; Fyfe, C. A.; Hartman, J. S. A Reexamination of Si, Al Ordering in Zeolites NaX and NaY. *J. Chem. Soc., Faraday Trans. 2* **1982**, *78*, 1025−1050.
(51) Lippmaa, E.; Magi, M.; Samoson, A.; Tarmak, M.; Engelhardt, G. Investigation of the Structure of Zeolites by Solid-State High-Resolution ^{29}Si NMR Spectroscopy. *J. Am. Chem. Soc.* **1981**, *103*, 4992−4996.
(52) Melchior, M. T.; Vaughan, D. E. W.; Jacobson, A. J. Characterization of the Silicon Aluminum Distribution in Synthetic Faujasites by High-Resolution Solid-State ^{29}Si NMR. *J. Am. Chem. Soc.* **1982**, *104*, 4859−4864.
(53) Dedecek, J.; Sklenak, S.; Li, C.; Wichterlova, B.; Gabova, V.; Brus, J.; Sierka, M.; Sauer, J. Effect of Al-Si-Al and Al-Si-Si-Al Pairs in the ZSM-5 Zeolite Framework on the ^{27}Al NMR Spectra. A Combined High-Resolution ^{27}Al NMR and DFT/MM Study. *J. Phys. Chem. C* **2009**, *113*, 1447−1458.
(54) Fyfe, C. A.; Gobbi, G. C.; Kennedy, G. J. Investigation of the Conversion (Dealumination) of ZSM-5 into Silicalite by High-Resolution Solid-State ^{29}Si and ^{27}Al MAS NMR Spectroscopy. *J. Phys. Chem.* **1984**, *88*, 3248−3253.
(55) Dedecek, J.; Kaucky, D.; Wichterlova, B. Co^{2+} Ion Siting in Pentasil-Containing Zeolites, Part 3. Co^{2+} Ion Sites and their Occupation in ZSM-5: A vis Diffuse Reflectance Spectroscopy Study. *Microporous Mesoporous Mater.* **2000**, *35*−*36*, 483−494.
(56) Dedecek, J.; Wichterlova, B. Co^{2+} Ion Siting in Pentasil-Containing Zeolites. I. Co^{2+} Ion Sites and their Occupation in Mordenite. A vis-NIR Diffuse Reflectance Spectroscopy Study. *J. Phys. Chem. B* **1999**, *103*, 1462−1476.
(57) Drozdova, L.; Prins, R.; Dedecek, J.; Sobalik, Z.; Wichterlova, B. Bonding of Co Ions in ZSM-5, Ferrierite, and Mordenite: An X-Ray Absorption, UV-vis, and IR Study. *J. Phys. Chem. B* **2002**, *106*, 2240−2248.
(58) Kaucky, D.; Dedecek, J. I.; Wichterlova, B. Co^{2+} Ion Siting in Pentasil-Containing Zeolites. II. Co^{2+} Ion Sites and their Occupation in Ferrierite. A vis Diffuse Reflectance Spectroscopy Study. *Microporous Mesoporous Mater.* **1999**, *31*, 75−87.
(59) Sobalik, Z.; Dedecek, J.; Kaucky, D.; Wichterlova, B.; Drozdova, L.; Prins, R. Structure, Distribution, and Properties of Co Ions in Ferrierite Revealed by FTIR, UV-vis, and EXAFS. *J. Catal.* **2000**, *194*, 330−342.
(60) Mortier, W. J.; Pluth, J. J.; Smith, J. V. Positions of Cations and Molecules in Zeolites with Mordenite-Type Framework. I. Dehydrated Ca-Exchanged Ptilolite. *Mater. Res. Bull.* **1975**, *10*, 1037−1045.
(61) Ogura, M.; Itabashi, K.; Dedecek, J.; Onkawa, T.; Shimada, Y.; Kawakami, K.; Onodera, K.; Nakamura, S.; Okubo, T. Stabilization of Bare Divalent Fe(II) Cations in Al-Rich Beta Zeolites for Superior NO Adsorption. *J. Catal.* **2014**, *315*, 1−5.
(62) Kresse, G.; Hafner, J. Ab-Initio Molecular-Dynamics for Open-Shell Transition-Metals. *Phys. Rev. B: Condens. Matter Mater. Phys.* **1993**, *48*, 13115−13118.
(63) Kresse, G.; Hafner, J. Ab-Initio Molecular-Dynamics Simulation of the Liquid-Metal Amorphous-Semiconductor Transition in Germanium. *Phys. Rev. B: Condens. Matter Mater. Phys.* **1994**, *49*, 14251−14269.
(64) Kresse, G.; Furthmuller, J. Efficient Iterative Schemes for Ab Initio Total-Energy Calculations Using a Plane-Wave Basis Set. *Phys. Rev. B: Condens. Matter Mater. Phys.* **1996**, *54*, 11169−11186.
(65) Kresse, G.; Furthmuller, J. Efficiency of Ab-Initio Total Energy Calculations for Metals and Semiconductors Using a Plane-Wave Basis Set. *Comput. Mater. Sci.* **1996**, *6*, 15−50.
(66) Klein, P.; Dedecek, J.; Thomas, H. M.; Whittleton, S. R.; Pashkova, V.; Brus, J.; Kobera, L.; Sklenak, S. NMR Crystallography of Monovalent Cations in Inorganic Matrixes: Li^+ Siting and the Local Structure of Li^+ Sites in Ferrierites. *Chem. Commun.* **2015**, *51*, 8962−8965.
(67) Sklenak, S.; Dedecek, J.; Li, C.; Wichterlova, B.; Gabova, V.; Sierka, M.; Sauer, J. Aluminum Siting in Silicon-Rich Zeolite Frameworks: A Combined High-Resolution ^{27}Al NMR Spectroscopy and Quantum Mechanics/Molecular Mechanics Study of ZSM-5. *Angew. Chem., Int. Ed.* **2007**, *46*, 7286−7289.
(68) Sklenak, S.; Dedecek, J.; Li, C.; Gao, F.; Jansang, B.; Boekfa, B.; Wichterlova, B.; Sauer, J. Aluminum Siting in the ZSM-22 and Theta-1 Zeolites Revisited: A QM/MM Study. *Collect. Czech. Chem. Commun.* **2008**, *73*, 909−920.
(69) Dedecek, J.; Sklenak, S.; Li, C. B.; Gao, F.; Brus, J.; Zhu, Q. J.; Tatsumi, T. Effect of Al/Si Substitutions and Silanol Nests on the Local Geometry of Si and Al Framework Sites in Silicone-Rich Zeolites: A Combined High Resolution ^{27}Al and ^{29}Si NMR and Density Functional Theory/Molecular Mechanics Study. *J. Phys. Chem. C* **2009**, *113*, 14454−14466.
(70) Brus, J.; Kobera, L.; Schoefberger, W.; Urbanova, M.; Klein, P.; Sazama, P.; Tabor, E.; Sklenak, S.; Fishchuk, A. V.; Dedecek, J. Structure of Framework Aluminum Lewis Sites and Perturbed Aluminum Atoms in Zeolites as Determined by $^{27}Al^{1}\{H\}$ Redor (3Q) MAS NMR Spectroscopy and DFT/Molecular Mechanics. *Angew. Chem., Int. Ed.* **2015**, *54*, 541−545.
(71) Klein, P.; Pashkova, V.; Thomas, H. M.; Whittleton, S. R.; Brus, J.; Kobera, L.; Dedecek, J.; Sklenak, S. Local Structure of Cationic Sites in Dehydrated Zeolites Inferred from ^{27}Al Magic-Angle Spinning NMR and Density Functional Theory Calculations. A Study on Li-, Na-, and K-Chabazite. *J. Phys. Chem. C* **2016**, *120*, 14216−14225.
(72) Whittleton, S. R.; Vicente, A.; Fernandez, C.; Rastegar, S. F.; Fishchuk, A. V.; Sklenak, S. Effect of Ge/Si Substitutions on the Local Geometry of Si Framework Sites in Zeolites: A Combined High Resolution ^{29}Si MAS NMR and DFT/MM Study on Zeolite Beta Polymorph C (BEC). *Microporous Mesoporous Mater.* **2018**, *267*, 124−133.
(73) VandeVondele, J.; Krack, M.; Mohamed, F.; Parrinello, M.; Chassaing, T.; Hutter, J. Quickstep: Fast and Accurate Density Functional Calculations Using a Mixed Gaussian and Plane Waves Approach. *Comput. Phys. Commun.* **2005**, *167*, 103−128.
(74) The cp2k program. https://www.cp2k.org (accessed October 25, 2018).
(75) Becke, A. D. Density-Functional Exchange-Energy Approximation with Correct Asymptotic-Behavior. *Phys. Rev. A: At., Mol., Opt. Phys.* **1988**, *38*, 3098−3100.
(76) Lee, C. T.; Yang, W. T.; Parr, R. G. Development of the Colle-Salvetti Correlation-Energy Formula into a Functional of the Electron-Density. *Phys. Rev. B: Condens. Matter Mater. Phys.* **1988**, *37*, 785−789.
(77) Hartwigsen, C.; Goedecker, S.; Hutter, J. Relativistic Separable Dual-Space Gaussian Pseudopotentials from H to Rn. *Phys. Rev. B: Condens. Matter Mater. Phys.* **1998**, *58*, 3641−3662.

DOI: 10.1021/acs.jpcc.8b07343
J. Phys. Chem. C 2019, 123, 7968−7987

(78) Krack, M. Pseudopotentials for H to Kr Optimized for Gradient-Corrected Exchange-Correlation Functionals. *Theor. Chem. Acc.* **2005**, *114*, 145−152.
(79) Wolinski, K.; Hinton, J. F.; Pulay, P. Efficient Implementation of the Gauge-Independent Atomic Orbital Method for NMR Chemical-Shift Calculations. *J. Am. Chem. Soc.* **1990**, *112*, 8251−8260.
(80) Frisch, M. J.; Trucks, G. W.; Schlegel, H. B.; Scuseria, G. E.; Robb, M. A.; Cheeseman, J. R.; Scalmani, G.; Barone, V.; Mennucci, B.; Petersson, G. A., et al. *Gaussian 09*, Revision C.01; Gaussian, Inc.: Wallingford, CT, 2011.
(81) Becke, A. D. Density-Functional Thermochemistry. III. The Role of Exact Exchange. *J. Chem. Phys.* **1993**, *98*, 5648−5652.
(82) Jensen, F. Basis Set Convergence of Nuclear Magnetic Shielding Constants Calculated by Density Functional Methods. *J. Chem. Theory Comput.* **2008**, *4*, 719−727.
(83) Benco, L.; Bucko, T.; Grybos, R.; Hafner, J.; Sobalik, Z.; Dedecek, J.; Hrusak, J. Adsorption of NO in Fe^{2+}-Exchanged Ferrierite. A Density Functional Theory Study. *J. Phys. Chem. C* **2007**, *111*, 586−595.
(84) Benco, L.; Bucko, T.; Grybos, R.; Hafner, J.; Sobalik, Z.; Dedecek, J.; Sklenak, S.; Hrusak, J. Multiple Adsorption of NO on Fe^{2+} Cations in the Alpha- and Beta-Positions of Ferrierite: An Experimental and Density Functional Study. *J. Phys. Chem. C* **2007**, *111*, 9393−9402.
(85) http://www.iza-online.org/synthesis/Recipes/SSZ-13.html (accessed October 25, 2018).
(86) Akporiaye, D. E.; Dahl, I. M.; Mostad, H. B.; Wendelbo, R. Aluminum Distribution in Chabazite: An Experimental and Computational Study. *J. Phys. Chem.* **1996**, *100*, 4148−4153.
(87) Itakura, M.; Goto, I.; Takahashi, A.; Fujitani, T.; Ide, Y.; Sadakane, M.; Sano, T. Synthesis of High-Silica CHA Type Zeolite by Interzeolite Conversion of FAU Type Zeolite in the Presence of Seed Crystals. *Microporous Mesoporous Mater.* **2011**, *144*, 91−96.
(88) Mackenzie, K. J. D.; Smith, M. E. *Multinuclear Solid State NMR of Inorganic Materials*; Elsevier, 2002.
(89) Kuriyavar, S.; Bortnovsky, O.; Tvaruzkova, Z.; Sobalik, Z. FTIR Study of Metal Zeolites. Determination of Co(II) Cation in Co-Beta Zeolite by Deuterated Acetonitrile Adsorption. *Collect. Czech. Chem. Commun.* **2001**, *66*, 685−692.
(90) McCusker, L. B.; Seff, K. Crystal-Structures of Hydrated and Partially Dehydrated Fully Cadmium(II)-Exchanged Zeolite A. *J. Phys. Chem.* **1981**, *85*, 166−174.
(91) McCusker, L. B.; Seff, K. Crystal-Structures of Fully Zinc(II)-Exchanged Zeolite A, Hydrated and Partially Dehydrated at 600 Degrees C. *J. Phys. Chem.* **1981**, *85*, 405−410.
(92) Mortier, W. J.; Pluth, J. J.; Smith, J. V. Positions of Cations and Molecules in Zeolites with Chabazite Framework. I. Dehydrated Ca-Exchanged Chabazite. *Mater. Res. Bull.* **1977**, *12*, 97−102.
(93) Mortier, W. J.; Pluth, J. J.; Smith, J. V. Positions of Cations and Molecules in Zeolites with Chabazite Framework. III. Dehydrated Na-Exchanged Chabazite. *Mater. Res. Bull.* **1977**, *12*, 241−249.
(94) Verberckmoes, A. A.; Weckhuysen, B. M.; Pelgrims, J.; Schoonheydt, R. A. Diffuse-Reflectance Spectroscopy of Dehydrated Cobalt-Exchanged Faujasite-Type Zeolites - a New Method for Co^{2+} Siting. *J. Phys. Chem.* **1995**, *99*, 15222−15228.
(95) Verberckmoes, A. A.; Weckhuysen, B. M.; Schoonheydt, R. A. Spectroscopy and Coordination Chemistry of Cobalt in Molecular Sieves. *Microporous Mesoporous Mater.* **1998**, *22*, 165−178.
(96) Klier, K.; Kellerman, R.; Hutta, P. J. Spectra of Synthetic Zeolites Containing Transition-Metal Ions. V. *Pi-Complexes of Olefins and Acetylene with Co(II)A Molecular-Sieve. *J. Chem. Phys.* **1974**, *61*, 4224−4234.
(97) Klier, K. Stereospecific Adsorption of Nitrous Oxide, Cyclopropane, Water, and Ammonia on Co(II)A Synthetic Zeolite. *Adv. Chem. Ser.* **1971**, *101*, 480−489.

DOI: 10.1021/acs.jpcc.8b07343
J. Phys. Chem. C 2019, 123, 7968−7987